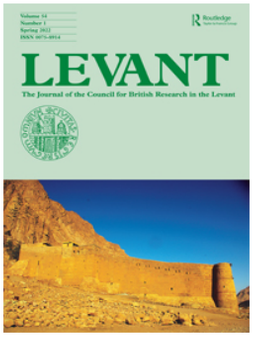

Routledge
Taylor & Francis Group

Levant

The Journal of the Council for British Research in the Levant

ISSN: (Print) (Online) Journal homepage: https://www.tandfonline.com/loi/ylev20

# Raincheck: A new diachronic series of rainfall maps for Southwest Asia over the Holocene

Zarina Hewett, Michelle de Gruchy, Daniel Hill & Dan Lawrence

**To cite this article:** Zarina Hewett, Michelle de Gruchy, Daniel Hill & Dan Lawrence (2022) Raincheck: A new diachronic series of rainfall maps for Southwest Asia over the Holocene, Levant, 54:1, 5-28, DOI: 10.1080/00758914.2022.2052660

**To link to this article:** https://doi.org/10.1080/00758914.2022.2052660

# Raincheck: A new diachronic series of rainfall maps for Southwest Asia over the Holocene

**Zarina Hewett [1], Michelle de Gruchy [1], Daniel Hill [2] and Dan Lawrence [1]**

Fluctuations in climate have been associated with significant societal changes, both in the modern day and in the past. In dryland environments such as much of Southwest Asia, rainfall is often used as a proxy for soil moisture available for crop production, and in pre-industrial societies this is assumed to directly relate to food production capacity and security. However, rainfall values are commonly quoted in archaeological literature without further context. Variability between values arising from different methods and timescales are rarely considered. This is important as small changes in rainfall can have profound effects on the interpretation of sites and landscapes. Here, we present a novel set of snapshot precipitation maps for Southwest Asia between the years 10,240 BP and 300 BP, based on previously published natural archive data by Bar-Matthews and Ayalon (2004) from Soreq Cave, and a newly derived modern rainfall map. The modern map was created using station data from the years 1960–1990 and a geostatistical interpolation technique applied across 14 separate zones. We outline the steps involved in the creation of the maps and provide access to, and clear explanations of, the data and methods used. Using the hindcasted maps, two case studies to highlight why a nuanced approach to rainfall is required in the study of ancient societies are examined. Changes to the spatial extent of the so-called 'Zone of Uncertainty' through time, as well as land suitable for rainfed agriculture throughout time using a simple model are calculated. It is demonstrated that relatively small fluctuations in rainfall can have a significant impact on the distribution of moisture availability for the region. It is argued that archaeologists need to be aware of the sources and limitations of the rainfall data used in their interpretations, and our map series is offered as a baseline dataset.

**Keywords** rainfall, precipitation, Middle East, Near East, climate change

## Introduction

Southwest Asia is dominated by dryland environments (Zohary 1973). Over the course of the Holocene, the region experienced a series of significant social transformations, including the emergence of farming societies and the endogenous development of cities, states and empires (Lawrence and Wilkinson 2015; Lawrence *et al.* 2017; Ur 2010; Yasur-Landau *et al.* 2018). Climate changes, and especially shifts in rainfall, have been seen as a significant factor in social changes (e.g., Dalfes 1997; Faust and Ashkenazy 2007; Fuks *et al.* 2017; Kaniewski *et al.* 2012; Kennett and Kennett 2006; Maher *et al.* 2011; Ur 2015; Weiss *et al.* 1993; Wossink 2009). Fluctuations in rainfall are generally (and often implicitly) used as a proxy for soil moisture available for crop production, and in pre-industrial societies this is assumed to directly relate to food production capacity and security. In the short term, 'collapse' events brought about by extreme weather changes such as droughts have been posited as causally

[1]Archaeology Department, Durham University, Durham, UK; [2]School of Earth and Environment, University of Leeds, Leeds, UK

Dan Lawrence (corresponding author), Archaeology Department, Durham University, Durham, UK. Email: dan.lawrence@durham.ac.uk


DOI 10.1080/00758914.2022.2052660

linked to declines in population, social complexity and specific political systems (Kaniewski *et al.* 2015; Kirleis and Herles 2007; Kuzucuoğlu and Marro 2007; Weiss 2017; Weiss *et al.* 1993). Increased rainfall has also been posited as a factor behind ancient settlement in regions which today are considered marginal, such as parts of Neolithic Arabia (Groucutt *et al.* 2020) or the so-called 'Zone of Uncertainty' at the interface of steppe and agricultural landscapes in the Northern Fertile Crescent (Smith *et al.* 2014; Wilkinson *et al.* 2014). More broadly, relationships between the environment, population levels and productive capacity are important for models describing the development of urbanism and hierarchical political systems (e.g. Algaze 2008) and in debates over the long term sustainability of complex societies (Lawrence *et al.* 2016; Palmisano *et al.* 2021).

Despite their critical importance to models of past social change, research on ancient rainfall patterns at scales relevant for archaeological enquiry has been limited. In this paper, a new modern precipitation map for Southwest Asia, based on World Meteorological Organisation station data is presented and compared to other rainfall maps available. The study area extends north to south from the Caucasus and Arabia, and east to west from Anatolia to Iran. The modern map is then used to hindcast palaeorainfall data from 10,240 to 300 BP at irregular intervals, using data derived from isotopic analyses of deposits from Soreq Cave, Israel. This timescale extends the original rainfall time-series presented by Bar-Matthews and Ayalon (2004) by 3000 years, intersecting with the Sapropel 1 event but not going beyond it so that changes in Sea Surface Temperatures are kept to a minimum. However, such changes are still significant, and it is strongly recommended that map users proceed with caution for the years 10–7kya BP. The time period was chosen to maximise the potential of the maps, which are the only ones of their kind currently available. The hindcasted rainfall maps are provided in full in the supplementary materials, so that they may be referred to individually with confidence within the context of the larger, and highly variable, time-series.

In the archaeological literature, rainfall values are commonly expressed as isohyet lines of annual rainfall in millimetres at fixed intervals (100, 200, 300, etc). These are usually derived from precipitation maps of Southwest Asia based on modern rainfall values collected from weather stations across the region. The variation between maps is due to differences in the sample of modern rainfall data used (the stations and time spans sampled) and from the interpolation method applied to transform data points into continuous values. A commonly used rainfall map was produced by the *Tübinger Atlas des Vorderer Orient* (TAVO, map A IV 4) in 1984 and uses rainfall values collected between the 1950s and 1970s. Stations across the region with fewer than five years of records were excluded (Wolfer 1984). Pearson's coefficients were calculated to quantify annual variations in the data, and the average value from each station was used in the interpolation process for mapping the isohyets (Wolfer 1984). More recent maps by Rayne (2014: 151–61) and Kalayci (2013: 85–98) use monthly precipitation data from the Global Precipitation Climatology Centre (GPCC) collected between 1980/81 and 2010. Additionally, Kalayci incorporates modern rainfall data from the National Climatic Data Centre (NCDC). Both the GPCC and NCDC datasets post-date the data used to produce the TAVO map. This is important to acknowledge, because it means these datasets may differ for any of three reasons: (1) inter-annual variability, (2) inter-decadal variability, and (3) climate change (Sun *et al.* 2018). While Rayne (2014: 151–61) followed an interpolation method analogous to that used for the TAVO map, the results are slightly different due to the spatial and temporal differences in the underlying sample datasets. Kalayci (2013: 85–98) made use of a similar dataset to Rayne (2014: 151–61), but used different interpolation methods and produced a further variation of mapped precipitation in the region.

The magnitude of the differences between modern rainfall values and those of earlier periods, even during the relative stability of the Holocene, is sufficient to have an impact on human settlement and productive capacity. Rainfall maps of past time periods therefore require hindcasting modern rainfall data with the use of proxy data (Kalayci 2013: 99–105). While a wide range of proxy data is available for Southwest Asia that can distinguish whether a given period was wetter or drier than present (see Clarke *et al.* 2016; Jones *et al.* 2019), deriving absolute rather than relative precipitation values is more problematic. Research at Soreq Cave has correlated variations in oxygen and carbon isotope values in speleothems to quantified changes in annual rainfall (Bar-Matthews and Ayalon 2011; Bar-Matthews *et al.* 1997; 1998; Orland *et al.* 2014). These calculated changes can be integrated with the modern rainfall data to create a series of hindcasted maps of precipitation.

Ideally, other speleothem records with a wide and even spatial distribution should be included in the

calculation of palaeorainfall maps. Long term observations of rainfall amount and the isotopic composition of cave and rainwaters, along with analyses of the growth of contemporary speleothems, are required for similar palaeorainfall calculations to take place. Cave water content is highly dependent on the local climate, and the cave structure and environment, meaning that relationships between the water isotopic values are variable across the region. For example, Sofular Cave in north-western Turkey experiences intense rainfall with highly variable seasonality, making a relationship between rainfall amount and $\delta^{18}O$ values difficult to determine: in this case it was found that the carbon isotope $\delta^{13}C$ content was a better climate indicator (Göktürk *et al.* 2011), although further complications arise as significantly increased rainfall can lead to higher $\delta^{13}C$ (where we would expect lower values), as shorter residence times in the soil mean isotopic equilibrium is not reached. This highlights that there is no simple universal rule that can be applied to isotopic records of speleothems for the determination of the relationship between cave deposits and rainfall. Furthermore, speleothem records of $\delta^{18}O$ values in Southwest Asia have been shown to be particularly heterogeneous during key climate events of the Holocene, such as the later years of Sapropel 1 (~8.2kya BP to ~7kya BP) and in the last 2000 years during the Little Ice Age (Burstyn *et al.* 2019). An ideal set of hindcasted maps would be able to take these variations into account.

At a regional scale, small differences in the shape or location of an isohyet — modern or hindcasted — have little effect on the overall precipitation trends of the region. Indeed, broad spatial and temporal trends are well-known for Holocene Southwest Asia. Spatially, an arc of higher precipitation follows the foothills of the Taurus and Zagros Mountain ranges, enabling rainfed agriculture. Moving south within the arc of this region, often known as the Fertile Crescent, precipitation gradually falls, reaching minimal levels in northern Saudi Arabia. In Iran, the Zagros Mountains cast a rain shadow over the centre of the country, and a similar phenomenon effects the central highlands in Turkey. Generally, across the region coasts receive more precipitation, as do higher altitudes (Babu *et al.* 2011; Kalayci 2013; Rayne 2014; Wolfer 1984). Temporally through the Holocene, precipitation reached a maximum at about 6000 BP and has been gradually falling since (Amand *et al.* 2020; Bar-Matthews *et al.* 1997; Brayshaw *et al.* 2011; Cheng *et al.* 2015; Dean *et al.* 2018; Eastwood *et al.* 2007; Finné *et al.* 2011; Fleitmann *et al.* 2007; Migowski *et al.* 2006; Staubwasser and Weiss 2006; Stevens *et al.* 2006), although there is some regional variation (Jones *et al.* 2019).

For archaeologists, operating at more local scales, small differences in the precise shape or location of an isohyet can completely change how sites are interpreted. For example, crossing the threshold for sustainable rainfed agriculture could mean that large silos at a site are interpreted as local storage, while falling outside this zone the same structures could be taken as evidence of large-scale importation of grain in an arid environment dominated by pastoralism (Pfälzner 2002). These differences are then compounded when archaeologists aggregate these individual interpretations into a regional picture of settlement and society. This paper examines changes in precipitation over the duration of the Holocene, across Southwest Asia, including the Arabian Peninsula and Cyprus, informed by the sampling work at Soreq Cave. A reproduceable and open dataset of modelled rainfall values are provided (see online Supplemental Material), and the results using precipitation estimates from alternative sources of rainfall data, and a General Circulation Model (GCM) are assessed. The implications and possibilities of these results for Holocene settlement and crop productivity in a smaller region, the lowland, alluvial plains of Southwest Asia from the base of the foothills of the Taurus and Zagros Mountains to the northern fringes of the Arabian Peninsula, are then examined. The goals of the paper are to describe the construction of the new precipitation dataset, to assess its strengths and weaknesses and, through two case studies, to demonstrate why a nuanced and contextual approach to past rainfall is critical for archaeologists and others working on ancient societies in this region.

## Materials and methods

Our modern rainfall map was created using freely available, quality controlled CLIMAT station data provided by the World Meteorological Organisation (WMO) and the Deutscher Wetterdienst (DWD). The climatological normals (defined as thirty-year monthly averages) for the period 1961–1990 were used for the majority of stations, with additional stations added from rainfall values calculated from monthly data for the same period. The climatological normals for this period serve as a standard in long-term climate studies. However, they come with uncertainties such as (1) differences in instrumentation between stations, (2) changes in instrumentation at a station, and (3) changes in station location (DWD

Climate Data Center 2017a). The DWD climate normals are cross checked with national meteorological services before publication, but the original WMO normals have also been included to increase the station density. The monthly data, also provided by the DWD, consists of quality-controlled observations taken from national weather services around the world. The quality control includes a check for inconsistencies in the station reports, a check against climatological thresholds, an environmental check and a comparison with the wider network (DWD Climate Data Center 2017b). Years with complete observations were used to calculate the mean annual rainfall across the period. To ensure data quality while maximising the number and distribution of data points, stations were required to have at least five complete years of data. This resulted in a total of 244 stations being made available for the interpolation (14 separately calculated, 201 DWD climate normals and 29 WMO climate normals). Figure 1 shows the distribution of stations across the study region which extends from 25.4 to 63.4° longitude and 12.5 to 43.6° latitude. Stations from beyond this boundary were also considered in the interpolation process to avoid edge effects.

The choice of interpolation method is dependent on several factors, including 1) the time step of the study period, 2) orographic factors and 3) data availability. Previous studies have shown that including geographic and topographic features in regression-based interpolation methods can improve rainfall estimates in data-sparse regions (Chapman and Thornes 2003; Goovaerts 2000; Jacquin and Soto-Sandoval 2013; Kyriakidis *et al.* 2001). Where a study region passes through different climate regimes, such as a coastal area bounded by a rain shadow on the leeward side of a mountain range, it can also be useful to separate the region into different zones for the interpolation (Mmbando and Kleyer 2018; Thomas and Herzfeld 2004). The size, station distribution, topography and precipitation gradients expected across our study region mean this zonal approach is appropriate.

The mean annual rainfall for each station was used, along with elevation and distance to coast, to create the rainfall map by means of Universal Kriging (also known as Kriging with External Drift, KED). A Digital Elevation Model (DEM) at 30 m resolution derived from the Shuttle Radar Topography Mission (SRTM) was used for the elevation data. Since the study region is large and has a complex climate, the region was split into 14 zones which were all interpolated separately. The zones were established in QGIS and they accounted for differences in terrain and known climate behaviour (see below). As an initial target, each region was required to have at least ten stations involved in the interpolation, including those outside of the immediate interpolation area. Including stations from outside the interpolation area was important for matching neighbouring regions, based on the assumption that changes in rainfall between different regions would be somewhat smooth.

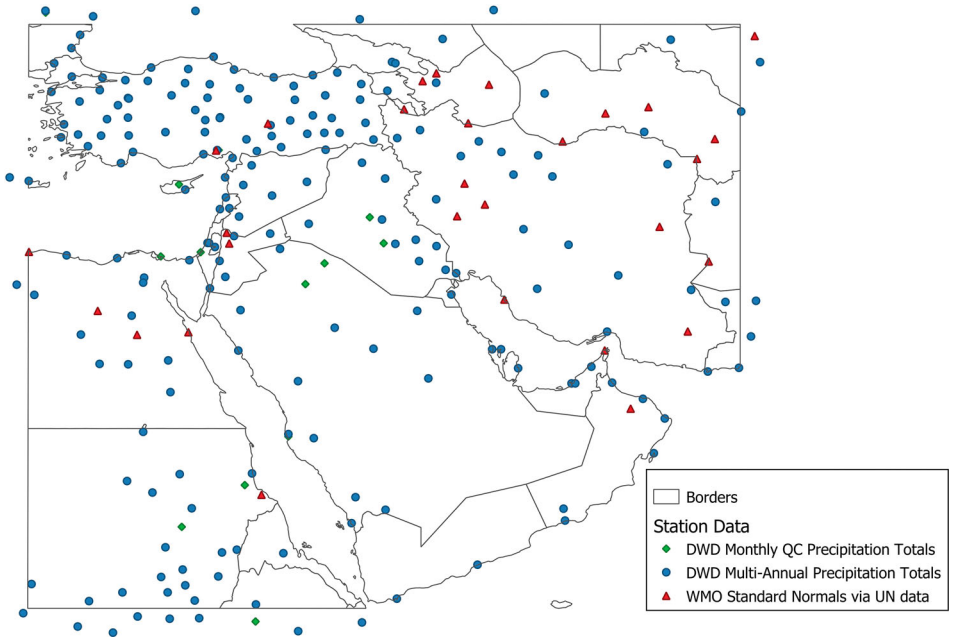


**Figure 1 Map of the study region showing the distribution of WMO weather stations, and the type of precipitation data used.**

For regression-based methods such as KED, variograms are used to determine the degree to which a set of data are spatially dependent. For example, two data points further apart have less spatial dependence than two that are closer together. Semi-variograms (sometimes just known as variograms) are used when there is another spatially independent variable, such as elevation, to interpolate over. By default, a spherical model was chosen, with elevation being the only secondary input. In regions where coastal proximity is known to be an important factor, this was included as a third interpolation input. If a spherical model would not fit the data, then an exponential or a gaussian model was tried instead.

### *Region justifications*

The decisions behind the division of individual regions can be explained according to the key topographical and climatological factors they exhibit. The regions are shown in Fig. 2.

Regions 1 and 2 cover eastern Africa and the Arabian Peninsula, which were split across the middle to form northern and southern regions. For the southern region (1), at the south-western edge of the Arabian Peninsula, rainfall can occur year-round due to interactions with African and Mediterranean airflows combined with orographic effects, particularly in summer when monsoon conditions dominate (Subyani 2004). Eritrea and northern Ethiopia also experience periods of heavy rainfall, with a large contribution arising from interactions with the Red Sea and moisture from the Mediterranean (Viste and Sorteberg 2013). Northern Ethiopia and Eritrea and the Southern Arabian Peninsula were included in the same interpolation zone as they both have areas that experience large amounts of rainfall where there is a strong relationship with elevation.

The northern part of region 2 is characterized by warm, dry summers, with winter and spring bringing storms from both the Mediterranean and the Red Seas (Patlakas *et al.* 2019). The distance to the Mediterranean Sea, which accounts for most precipitation across the region, was therefore used as a covariate for this region.

Two interpolation regions covered the area immediately south of the Taurus and Zagros mountains. One region followed the coastline of the Mediterranean Sea and was bounded by the Lebanon and Judean mountains to the east, and the Taurus range to the north (region 3). Another region covered a large area that included most of Syria and Iraq (region 4). The regions were separated to account for the rain shadow effect where moist air from the Mediterranean is carried upwards by the mountains, causing it to cool and fall on the windward side, therefore leaving less moisture to fall on the leeward side. As a result, Syria is mostly arid or semi-arid, but with wetter areas by the coast in the north-west.

Turkey, which has a varied climate heavily dependent on the terrain, was divided into smaller regions

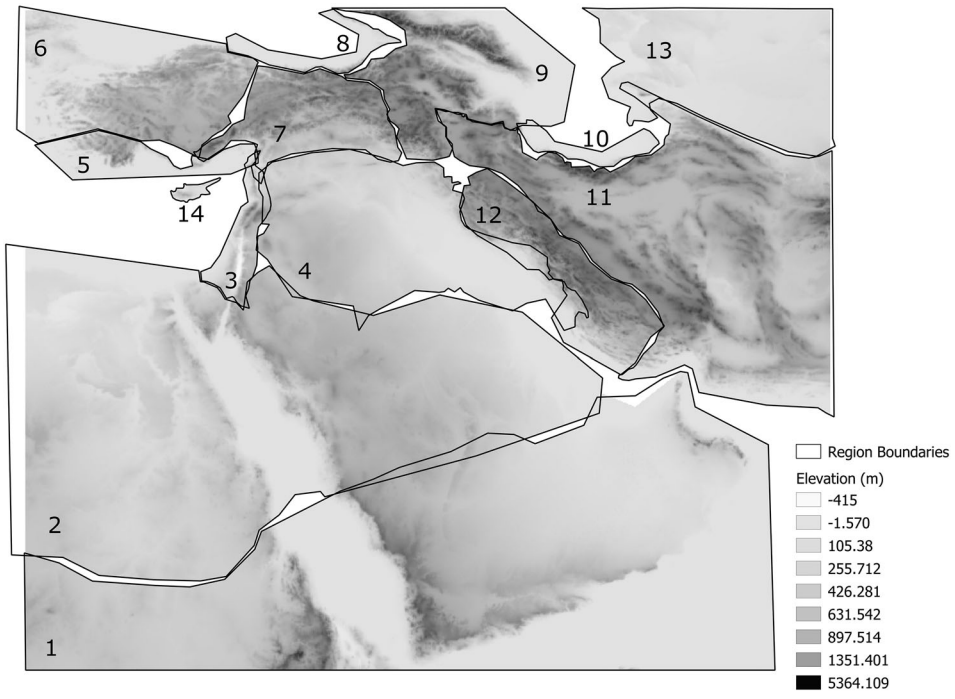


**Figure 2 Elevation map showing the 14 different interpolation zones.**

to avoid under-representing regional effects that arise due to large mountain chains. In creating this map, Turkey was split across five interpolation zones: the Mediterranean coastline (region 5), the Black Sea coastline (region 8), an area covering the Marmara and central Anatolian regions (region 6), and two areas covering eastern and south-eastern Anatolia which also stretch into the Armenian highlands and Caucasus mountains (regions 7 and 9). Previous studies have sought to define the climate zones of Turkey (Iyigun *et al.* 2013; Sensoy *et al.* 2008) and these findings were used to inform the boundaries of the interpolation areas.

The distance to the Black Sea was used alongside elevation in regions 8 and 9. The south-eastern edge of the coastline is the wettest part of this and is also the only region in Turkey that experiences rainfall all year round. Rain falls mostly on the windward (northern) side of the mountains that line the coast, creating a rain shadow effect that is particularly prominent in central Anatolia, a region that has a variable steppe climate with low amounts of precipitation (usually in the form of snow). The Black Sea and Caucasian mountains experience a continental climate resulting in long and cold winters with frequent heavy snowfall (Sensoy *et al.* 2008).

The modern climate of the Caucasus region is dominated by westerlies that carry moisture from the Black and Mediterranean Seas. High pressure systems block storms entering from the north. The high elevation of the greater and lesser Caucasus mountains strongly impacts the regional climates, with windward (western) flanks receiving more precipitation. The region then gradually becomes more arid going eastwards towards the Caspian Sea (Borisov 1965; Forte *et al.* 2016).

In Iran, there is a more moderate and wetter climate along the coast of the Caspian Sea, before the peaks of the Alborz mountains block much of the moisture from entering the hot and dry interior. The salt deserts Dash-e Kavir and Dash-e Lut occupy the lowlands of the country, whilst further west the Zagros mountains introduce a colder and wetter climate resulting from incoming moisture from the Mediterranean Sea. For the interpolation, this area was mostly covered by three regions: one for the coastal areas by the Caspian Sea (region 10), one for inland areas including the Alborz mountains and the desert areas (region 11), and one for the Zagros mountains (region 12). Region 4, which covered most of Iraq and Syria, also includes the south-western corner of Iran up to the Persian Gulf.

Region 13 covered the area north of the Alborz mountains, including most of Turkmenistan. This area had a low station density and was the only area where the target of ten stations could not be met and stations from neighbouring regions could not aid the model. As well as having a low station density, this region also has less varied terrain and is flatter by comparison to other areas in the study region, which makes a similar elevation-based model more difficult to fit. A singular model was used based on previous studies and observations of the distribution of precipitation. Turkmenistan has a continental and cold-desert climate, with three times the amount of rainfall occurring in the winter months compared to the summer. The highest amount of rainfall occurs in the Kopet Dag range that joins with the Alborz in the south of the country (Orlovsky 1994), which was included in the interpolation region centred on inland Iran.

The 14th and final region covered Cyprus. There were only two stations on Cyprus that featured in the interpolation, so points from the coastlines of the mainland were also used.

Further steps were involved in the map creation. First, to avoid harsh edge effects at the boundaries between interpolation areas, gaps were left between some regions which were then filled by nearest neighbour interpolation. At other times, isohyet matching could be used when overlapping areas contained similar values. Once all zones had been interpolated, the separate areas were then joined using mosaicking by averages. The final step was to replace negative values that arose as a result of interpolation in highly arid areas with zeros — this happened in only three areas: Dasht-e Lut in Iran, an area south of the Dead Sea in the Jordan Rift Valley, and in parts of the Western Desert in Egypt.

### *Hindcasting*

Soreq Cave is part of a series of karstic caves located in the Judean Hills approximately 40 km inland from the Mediterranean Sea. The caves have been the subject of a series of studies in palaeoclimatology since they were opened by quarrying in 1968 (Bar-Matthews and Ayalon 2004; Bar-Matthews *et al.* 1997; 1998; 2000; Orland *et al.* 2009; 2012; 2019), and long-term observations and constant environmental conditions have provided a continuous palaeoclimate record of the past 125kya BP for the eastern Mediterranean region. Bar-Matthews and Ayalon (2004) calculated past annual rainfall values from the measurements of stable isotope $\delta^{18}O$ and $\delta^{13}C$ contained within cave deposits. Close monitoring of the $\delta D$ and $\delta^{18}O$ content of cave drip waters showed that these isotope values decrease with increased

rainfall, and that the modern rainfall values follow the Mediterranean Meteoric Water Line (MMWL).

Continuous observations of rainfall and isotope content between the years 1990–2007 indicate that the average annual rainfall at the site is between 500 and 600 mm, with approximately 95% of this occurring between November and April. Precipitation was found to be related to its $\delta^{18}O$ amount by the equation:

$$\text{Annual Rainfall (mm)} = \frac{-3.9 - \delta^{18}O\ (_0/_{00},\ VSMOW)}{0.0039} \quad (1)$$

whereby an increase of $\delta^{18}O$ values by 1‰ corresponds to approximately 280 mm less rainfall per year (Orland *et al.* 2009). Orland produced an updated version of the transformation equation originally found in Bar-Matthews and Ayalon's 2004 paper (seen in fig. 4 of that paper), using the additional years of rainfall up to 2007. This led to a decreased R value (0.91 to 0.70) which was attributed to the natural variability of rainfall on short (decadal) timescales. This was not deemed a significant reason to not use the later equation, although this would increase uncertainty in the precipitation estimates. When applied to the $\delta^{18}O$ values of speleothem sample 2-N the rainfall values from the past 10kya BP years could be derived, and this result is shown in Fig. 3. The data from these results were used to create hindcasted maps of rainfall back to 10kya BP at intervals matching those of the temporal availability of the 2-N speleothem data.

The method of hindcasting was determined by analysing the variability of annual rainfall in wet and dry areas. The range in rainfall values was compared to the annual average for each station to assess whether, a simple addition and subtraction, or proportional methods, were most appropriate (see below). This approach also allows us to comment on the degree to which proportional changes could be generalized across the region, and to identify areas where it would be more or less effective.

## Results

The final modern map is shown in Fig. 4. Out of the 14 regions, two of the models were exponential and another two were gaussian. A summary of the interpolation regions is given in Table 1.

An example semi-variogram for region 1 is shown in Fig. 5. As one might expect, the variability between precipitation values increases with distance until it reaches a plateau (or sill), where there is no further identifiable spatial correlation. Note that there is much variation around the model, which is most likely an effect of having low station densities. Full details on the individual models, their semi-variograms, and example R code are provided in the Supplemental Material.

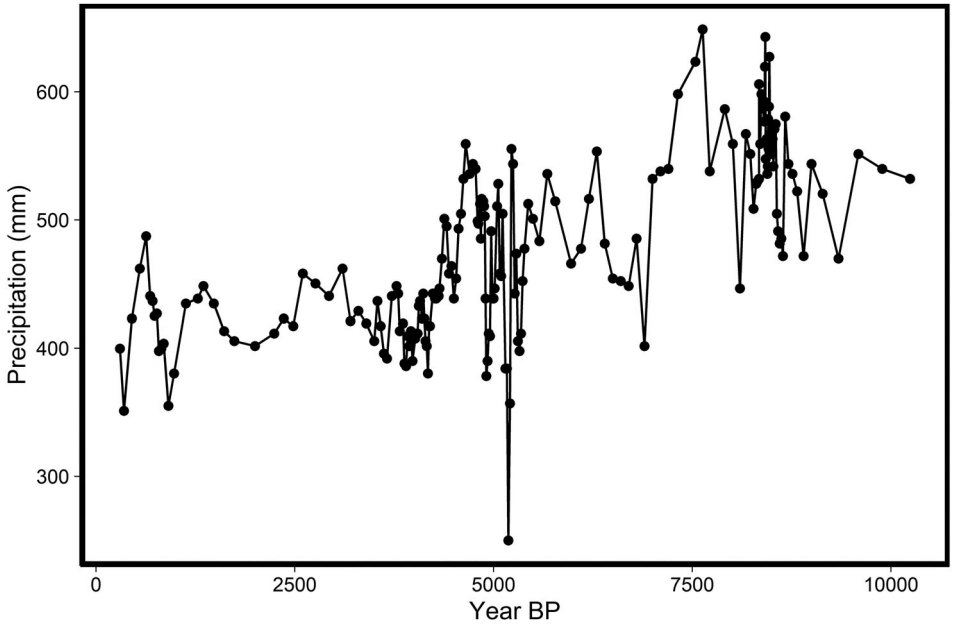


**Figure 3 Palaeorainfall at Soreq Cave, Israel, calculated from $\delta^{18}O$ isotope data originally published by Bar-Matthews and Ayalon (2004).**

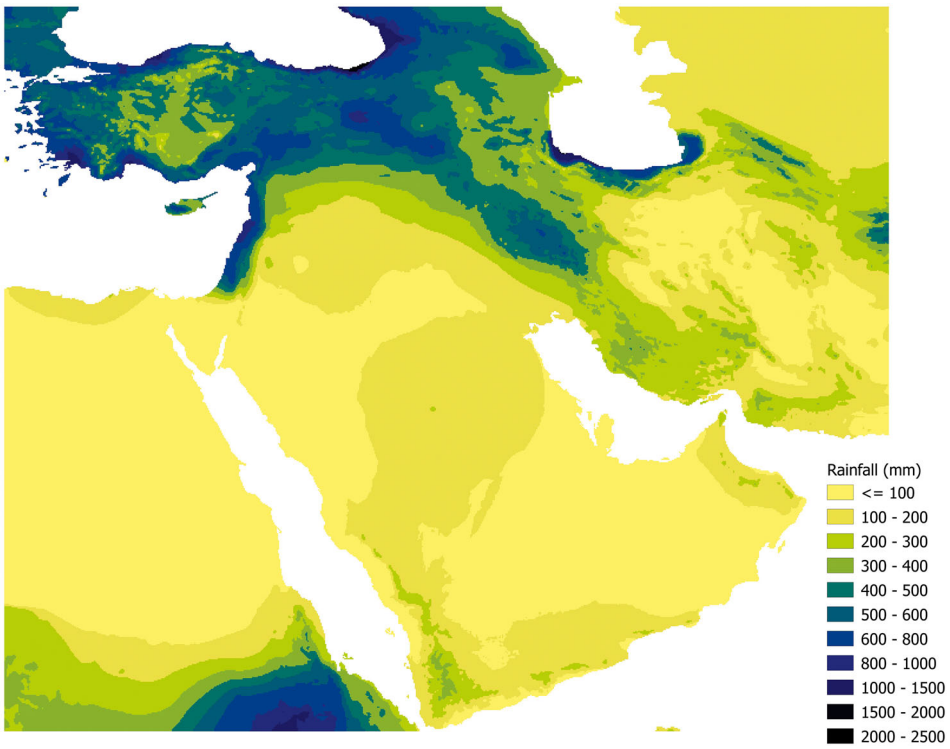


**Figure 4** **Modern rainfall map created via a regional regression-based kriging method with WMO station data.**

**Table 1** **Information on each of the interpolation zones used to create the modern precipitation map**

| Label Number | Name of zone | Cropped station density (per degree$^2$) | Type of model | Covariates |
|---|---|---|---|---|
| 1 | AP_SOUTH_ERITREA | 0.107 | Spherical | Elevation |
| 2 | NORTH_AP_EGY | 0.115 | Spherical | Elevation, distance to coast (Mediterranean) |
| 3 | EAST_MED | 1.542 | Spherical | Elevation, distance to coast (Mediterranean) |
| 4 | IRAQ_SYRIA | 0.271 | Spherical | Elevation |
| 5 | TURKEY_MED | 0.433 | Spherical | Elevation |
| 6 | WEST_TURKEY | 0.510 | Spherical | Elevation |
| 7 | TAURUS | 0.572 | Exponential | Elevation |
| 8 | BLACKSEA | 0.578 | Exponential | Elevation, distance to coast (Black Sea) |
| 9 | CAUCASUS | 0.316 | Exponential | Elevation, distance to coast (Black Sea) |
| 10 | CASPIAN | 0.651 | Spherical | Elevation |
| 11 | IRAN_MAIN | 0.133 | Gaussian | Elevation |
| 12 | ZAGROS | 0.154 | Gaussian | Elevation |
| 13 | TURKMENISTAN | 0.085 | Spherical (Singular) | Elevation |
| 14 | CYPRUS | 1.831 | Spherical | Elevation |

### *Comparisons to TAVO, WorldClim and GPCC data*

The new modern rainfall map has been created for the climate normal period between 1960 and 1990, which is used as a standard baseline in climate studies (World Meteorological Organisation 2017). The suitability of the new map can be assessed by comparing it to other maps that cover the same time period. Three such maps commonly referenced by archaeologists are: (1) map A IV of TAVO (which uses data between the 1950s and 1970s), (2) the WorldClim precipitation map (between 1970 and 2000), and (3) gridded GPCC precipitation data derived from data from 1891 to 2016.

Since the TAVO map presents rainfall as ranges within vector polygons, the new raster rainfall map was compared to the minimum, maximum and midpoint of the TAVO map's precipitation ranges. The midpoint version was found to be most similar to the new map, with a mean difference of -7.5 mm, meaning our model suggests a drier regional average, though not as dry as the minimum range of TAVO. Around 63% of the data fell within ±50 mm

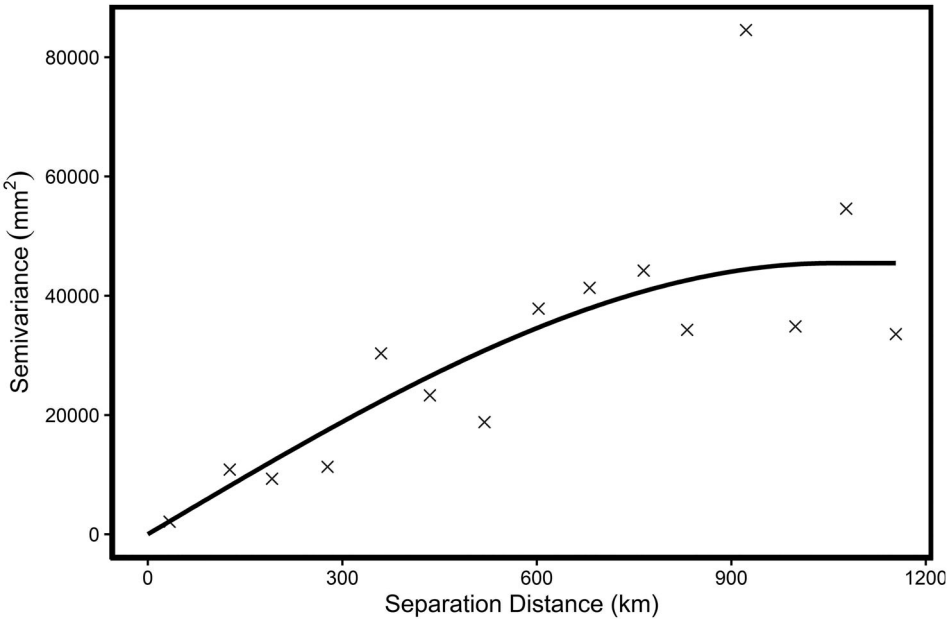


**Figure 5** **Semi-variogram for Region 1 (see Fig. 2), covering the southern part of the Arabian Peninsula and parts of eastern Africa. The separation distance is the distance between two points with units of km, whilst the semi-variance has units of mm$^2$.**

of the TAVO map, and 85% and 91% within 100 mm and 150 mm respectively, although there was a large range in variability with values reaching between -1400 mm and +650 mm. The areas that saw the biggest differences were those at high elevations or in coastal areas, regions which typically experience high levels of rainfall. These more extreme differences are likely due to the data made available to the interpolation method, with TAVO having a larger station density due to covering a different time period. This effect is most noticeable in Turkey, in the highlands by Antalya and Alanya by the Mediterranean Sea, where there is a gap in the distribution of WMO stations for this period. Contrastingly, in the south-east of Iran, where the station density is low in both cases, rainfall is higher in the new map by approximately 200 mm due to the inclusion of elevation in the interpolation.

Another widely used map, particularly in climate modelling studies, is the WorldClim climate surface for precipitation (Fick and Hijmans 2017). WorldClim provides spatially interpolated monthly climate data aggregated across the years 1970–2000. The maps cover all global land areas at a high spatial resolution (~ 1 km$^2$) using data from weather stations. The interpolation method consisted of using thin-plate splines along with a number of co-variates: elevation, distance to coast and satellite data, including maximum and minimum land surface temperatures and cloud cover. The best models for each region and variable were chosen for the final product, rather than using one model for the whole world. Whilst producing a higher resolution product than the GPCC derived maps, the accuracy of the WorldClim precipitation map was found to be only marginally improved with the addition of satellite data, and in some cases worsened it, with systematic errors (such as the over estimation of cloud cover) being carried over into the estimation of climate surfaces (Fick and Hijmans 2017; Wilson *et al.* 2014).

There are areas of our new rainfall map that are significantly drier than the WorldClim map, particularly in places that typically experience heavy rainfall. The mean difference for the whole region was -7.55 mm and the area with the largest difference in rainfall was in Georgia, at the coast of the Black Sea. It is likely that there is some under-estimation of rainfall here due to a lack of station points in the area, particularly at lower elevations near the coast. Our map also gives lower rainfall values at higher elevations in this region. It is possible that some of these differences are a result of over-estimation in rainfall by WorldClim, resulting from a systematic bias for cloud cover over high albedo land surfaces. This would be particularly relevant in mountainous areas in Turkey and the Caucasus, which experience significant snowfall in the winter months. Inaccuracies in higher elevation areas may also be the result of a systematic lack of stations in these areas (Hijmans *et al.* 2005). The other notable

difference between our map and the WorldClim precipitation surface is in the apparent sensitivity of rainfall to elevation across the Zagros mountains in Iran. Our map appears more sensitive, following a similar relationship to that displayed by more localized maps (for example Khalili and Rahimi 2014).

The GPCC monthly product provides monthly gridded precipitation maps stretching back to 1891. For the purposes of this comparison, the monthly data to yearly totals was summed and then averaged across the years 1960–1990, to match our temporal coverage. The product interpolates precipitation anomalies at stations using an empirical weighting method that has been adapted to a sphere (SPHEREMAP), and then superimposes this result with the GPCC Climatology v2018 map of the same resolution (in this case 0.25° x 0.25°) (Huffman *et al.* 2007; 2010). The GPCC map is wetter, with our map having a mean difference of -9.8 mm and a maximum drier difference of -1523 mm, again by the Black Sea. About 69% of the differences have a magnitude of less than 50 mm, increasing to 87% and 93% for 100 mm and 150 mm respectively (Table 2).

Figure 6 shows the TAVO, WorldClim and GPCC maps and the differences with our new map. There are other precipitation maps available for the region, some focused on certain countries and others with global applications. Table 3 outlines some of the other available maps which have not been discussed here. Ultimately, the main point archaeologists and historians should be aware of is the variety in rainfall estimates, and how those estimates can change depending on the data used and the method applied in the interpolation. When quoting rainfall values, it is important to state the source of the value, i.e., which map has been used and why. Each map discussed here has its own strengths and weaknesses, which may change depending on the area of focus. Our map has the benefit of being both a higher resolution and dependent on fewer variables. Increasing variables can introduce systematic errors, such as the issue with satellite data discussed above. Our dataset also improves on the discrete nature of the TAVO map, making it more useful at local scales. Like other maps, however, it still suffers from low station densities. The authors of other maps have detailed further strengths and limitations of their own datasets (Hijmans *et al.* 2005; Schneider *et al.* 2018).

In addition to the variability between different rainfall maps it is important to consider the scale of variation in rainfall over time. High rainfall areas typically experience larger variations year to year. Figure 7 shows how the range size of precipitation values varies with the average rainfall at a station for the years 1960 to 1990. Variation rises sharply for rainfall at sites with an average between 0–200 mm, then continues to rise at a slower rate. In regions that receive an average of over 1000 mm of rain per year, the magnitude of the variation can be just as high with range sizes over 1000 mm. Inter-annual variability is important to consider for calculations on long-term soil moisture, and therefore crop productivity and management requirements, but also has important implications for hindcasting.

### *Hindcasting and palaeorainfall maps*

By investigating the relationship between mean annual rainfall and the year-to-year changes in rainfall at each station, it can be seen that stations that experience more rainfall experience larger variation (see Fig. 7). It is, therefore, better to hindcast by using a proportion-based method, rather than by adding absolute differences, as a proportion-based method will take account of these differences. This method is uncomplicated and is simply a multiplication of a set of values across the modern map, but it should be noted that this method keeps modern dry areas dry throughout the hindcast. For this reason, caution is recommended when using these maps in areas that receive under 100 mm of rainfall in our modern data. For each year of the hindcast, the ratio of the palaeorainfall and modern rainfall (set as 500 mm at Soreq Cave) was calculated and multiplied with the modern rainfall map to achieve the hindcasted rainfall maps. Figure 8 shows a selection of hindcasted maps for periods of high and low rainfall as recorded in the isotope data from Soreq

**Table 2 A quantitative summary of the TAVO, WorldClim, and GPCC precipitation maps discussed in this text in comparison to the new modern precipitation map**

| | Mean | Max | Min | % < 100 mm | % > 2000 mm | % of new map — other map within 50 mm |
|---|---|---|---|---|---|---|
| New Map | 203.1 | 2068.1 | 0 | 15.4 | 0.002 | — |
| TAVO (Midpoint) | | 2000–2500 | <100 | 49.2 | 0.02 | 62.9 |
| WorldClim | 211 | 2241 | 0 | 36.5 | 0.01 | 68.8 |
| GPCC | 218.3 | 2430.7 | 0 | 17.7 | 0.02 | 69.3 |

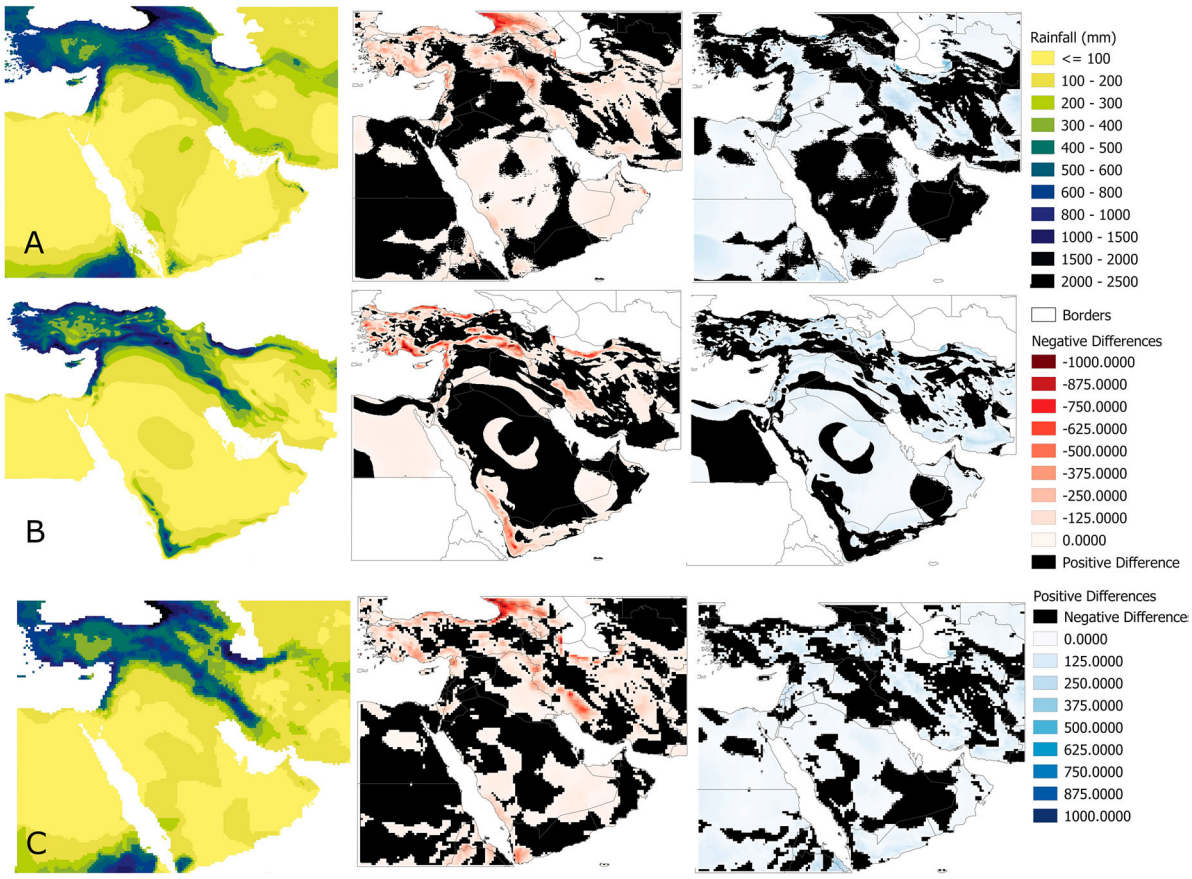


**Figure 6** **Maps used in previous studies compared against the new modern rainfall map derived in this study. Row A) WorldClim precipitation map, B) TAVO precipitation map, C) GPCC. The middle column shows the negative differences (where the new map was drier), and the last column shows the positive differences (where the new map was wetter).**

Cave, in order to demonstrate the degree of spatial fluctuations visible. Bar-Matthews and Ayalon 2004 discuss some of the main events in an archaeological context. These include a short period of low rainfall at 5.2kya BP, after which there is a quick recovery, which has been related to a period of social change by Weiss and Bradley (2001). Another long dry period occurs between 4.6–4.0kya BP, with rainfall values staying below the present-day average (between 500–600 mm) until late in the 20th century. deMenocal *et al.* (2000) attribute drying in North Africa and the Middle East around this time to earth orbital changes.

### *Hindcast-Model comparison*

To help assess our maps, the results are compared to a novel palaeoclimate simulation across our map region. This simulation is driven by the same forcings as previous simulations with the HadCM3 version of the Hadley Centre Unified Model (Cookson *et al.* 2019), but applied transiently between 5000 and 3000 years before present (BP), rather than in 250-year snapshots. Greenhouse gases are varied year on year, interpolating between the measurements of ice core records (Blunier *et al.* 1995; Flückiger *et al.* 2002; Monnin *et al.* 2004), while orbital parameters are adjusted every 50 years based on the orbital solutions (Laskar *et al.* 2004). The transient nature of this simulation allows us to temporally downsample the model data to match the time intervals of the Soreq Cave record and our hindcasted maps.

Absolute rainfall values differ between the model and the isotope data at the location of Soreq Cave, as would be expected due to the relatively low resolution of the model, which represents a much broader area and does not accurately reflect the topography of the region. However, if variation in the model relative to the pre-industrial value (530 mm/year) is compared to variation in the oxygen-isotope derived rainfall values relative to the most recent measurement (~390 mm/year), then a high level of agreement is seen, at least since ~4.2kya BP (see Fig. 9). The much larger precipitation changes seen in the Soreq Cave record between 5 and 4kya BP are

**Table 3 A summary of other available precipitation maps that cover Southwest Asia**

| Map Name | Data | Years | Resolution | Coverage | Method | Citations |
|---|---|---|---|---|---|---|
| A IV 4 in the *Tübinger Atlas des Vorderer Orient* (TAVO) | Stations with record duration of at least 5 years. | 1941–1977 | — | Middle East; 24.8° to 72.6°E, 12.1° to 42.1°N | Application of Pearson's coefficients to assess annual variations in data. Averages from stations were interpolated. | Alex and Stöehr (1985) |
| WorldClim | Station Data, Elevation, Coastal Distance, Cloud Cover. | 1970–2000 | 30s, 2.5 min, 5 min, 10 min available | Global | Thin Plate Splines, Regional model selection. | Fick and Hijmans (2017); Hijmans *et al.* (2005) |
| GPCC Full Data Monthly Product | ~80000 stations with record durations of at least 10 years | 1891–2016 | 0.25°, 0.5°, 0.75°, 1°, 2.5° | Global | Interpolation of anomalies with Shepard's empirical weighting across a spherical surface (SPHEREMAP). | Schneider *et al.* (2018) |
| Tropical Rainfall Measuring Mission (TRMM) Multi Satellite Precipitation Analysis TMPA (3B42) | Satellite observations with 'indirect' use of rain gauge data to rescale to monthly data. | 1998–2019 | 0.25° | -180°W to 180°E, 50°S to 50° N | Attributes rainfall to grid cells via combined analysis of microwave and infrared satellite estimates, then adjusts using rain gauge analysis. | Huffman *et al.* (2007); Huffman *et al.* (2010) |
| CPC Merged Analysis of Precipitation (CMAP) | Station data and precipitation estimates from satellite data. | 1979–Present | 2.5° | Global | Blending of gauge data with infrared and microwave satellite estimates. | Xie and Arkin (1997) |
| Iranian National Dataset (INDS) | Station data, elevation | 1961–2005 | 1 km | Iran | Correlation between rainfall and elevation, and application of a Kriging method for interpolation. | Khalili and Rahimi (2014) |
| IS0902 | Station data only (IRIMO stations) | 1998–2006 | 0.25° | Iran | Interpolation using Shepard's algorithm. | Javanmard *et al.* (2010); |
| CRU CL v 1.0 | Monthly climatological means for precipitation | 1961–1990 | 0.5° | All land areas (excluding Antarctica) | Interpolation using thin-plate splines and elevation. | New *et al.* (1999) |

not seen in this climate model simulation, which suggests that these changes may not have been forced by the orbital or greenhouse gas variations that drive these simulations. These changes in the Soreq Cave oxygen isotopes are associated with the largest excursions in carbon isotopes in the record of the last 6kya BP (Bar-Matthews and Ayalon 2004). While the carbon isotope changes may be a result of the precipitation changes, they could also reflect changes in the vegetation, soils or hydrology of the region (Fohlmeister *et al.* 2020).

To create a more robust image of the hindcast-model differences across the region, we took the log-transformed map of differences (where the difference was proportional and defined as hindcast/model) across the time period covered by the model. Figure 10 shows an example of this for the year 3100 BP. It is worth noting that spatial comparisons between the hindcasts and model simulations are hampered by differences in spatial resolutions.

The model appears to show very different levels of rainfall over large areas of our hindcast maps, however, there is good agreement in areas of the Levant and the Al-Jazira plain. Clearly, the Soreq Cave record is less relevant for changes in the climate of Arabia, Anatolia and the Zagros mountains, where significant differences are seen between the hindcast and model simulations. These areas are affected by Western Disturbances (Cookson *et al.* 2019) and changes in monsoonal rains (Jennings

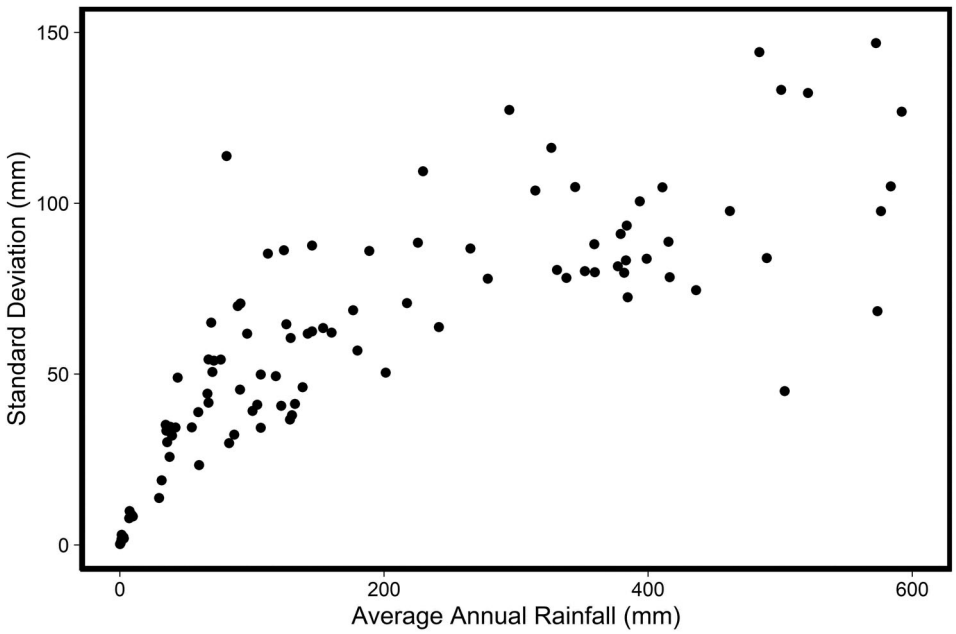


**Figure 7** **The range in precipitation values plotted against the corresponding average annual rainfall. The scale of variation increases with amount of rainfall.**

*et al.* 2015), which have little impact on the climate of the region around Soreq. However, it was decided to include these areas in the final product due to the absence of similar data for these regions. Hopefully when using these maps, researchers will be cautious and aware of the limitations stated here.

## Discussion

In this section some of the issues, essential for users of the maps to be aware of and understand when utilizing our rainfall data, are discussed.

The generalization of the Soreq Cave record across the whole of Southwest Asia is not ideal as palaeoclimate records tend to only reflect local scale climate, and other records in the region show heterogeneous behaviour at different times across the Holocene. Comparisons to other palaeoclimate proxies, in particular speleothems, highlight the spatial discrepancies between climate behaviour throughout the Holocene. Just as in modern times, the region's climate is varied and results from several complex systems such as those from the Mediterranean Sea, Black Sea and seasonal monsoon systems. The Soreq Cave isotopic record is shown to be tied to the Mediterranean Sea, but other speleothem records in other parts of the region show behaviour derived from other systems, as might be expected. For example, speleothem records from the Qunf and Hoti Caves in Oman, show a northward shift of the summer ITCZ during the early Holocene, followed by a gradual southern migration and decrease in monsoonal rainfall in the middle to late Holocene in response to solar insolation (Fleitmann *et al.* 2007). Sofular Cave in Turkey shows similar increased levels of precipitation to Soreq Cave and the eastern Mediterranean in the late to mid Holocene (Göktürk *et al.* 2011), but the authors highlight the discrepancies of the exact timings of the wet periods between different records throughout the region. Ideally, the palaeorainfall maps would include further rainfall proxy records where isotopic signatures have been converted to rainfall via their own specific rainfall transformation function, where there is a good understanding of the dominant source of moisture through time. This would allow the maps to better reflect regional climate changes through time.

The Soreq record itself has measurement uncertainties that also need to be considered. Exact values for the $\delta^{18}O$ uncertainties are often unpublished, but typical values are around 0.2‰ (Wassenaar *et al.* 2018). With this value, the estimated rainfall could vary by at least 55 mm, although this will increase when statistical uncertainty in the model and original rainfall data is taken to account. Uncertainties such as these could easily affect the way in which rainfall is interpreted at a location.

Another limitation to take into consideration are the age errors on the rainfall maps; which also tie directly to the age errors from the original Soreq Cave data. The methods used for deriving the $^{230}Th$ $^{234}U$ age estimates at Soreq Cave are detailed in

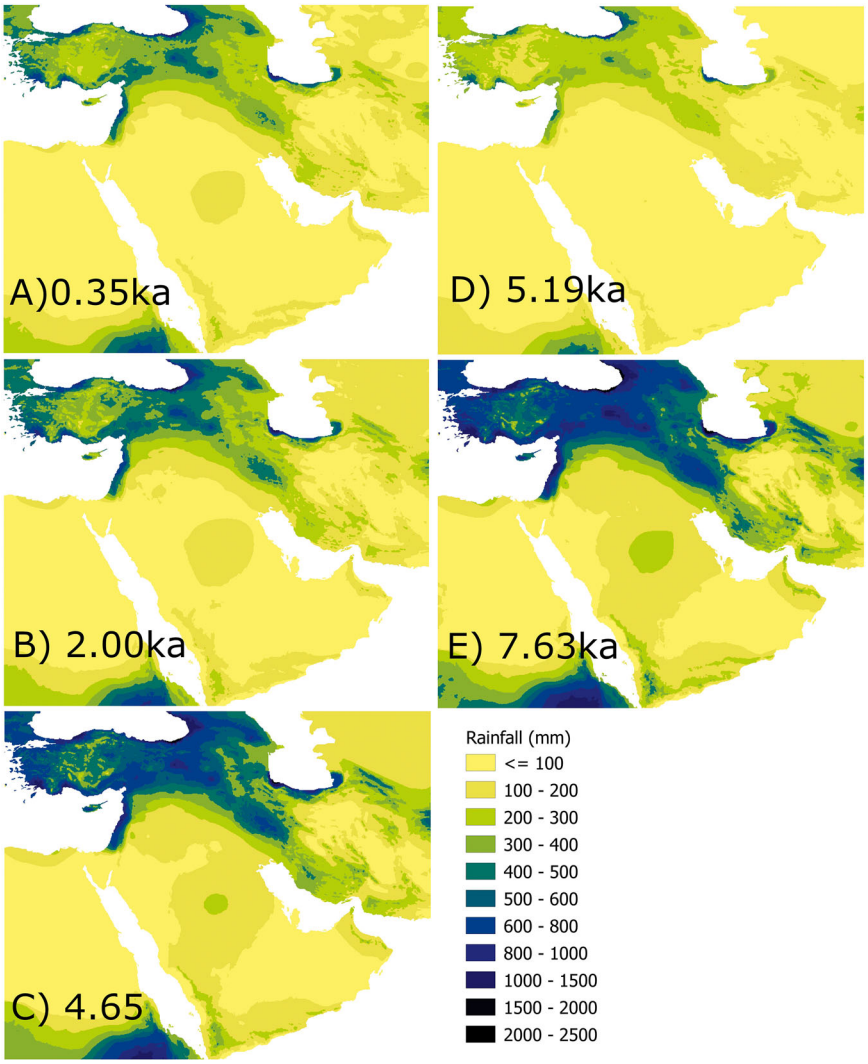


**Figure 8** **Selected hindcasted maps at key moments of high and low rainfall, as indcated by the Soreq Cave timeseries shown in Fig. 3.**

Kaufman *et al.* (1998) and for the speleothem sample 2N, used here, age estimate errors ranged between 340 and 1730 years. It is critical to consider these large uncertainties when trying to derive significance from the palaeorainfall record.

### *Case study: archaeological implications of rainfall shifts in the Fertile Crescent*

In this section the implications of spatial patterns in rainfall through time in the lowland alluvial plains of Southwest Asia, using the so-called 'Zone of Uncertainty' as a case study, are considered. The Zone of Uncertainty is defined as the area between the 180 mm and 300 mm isohyets, where rainfed agriculture is possible but risky, with precipitation in some years falling below that required to produce a viable cereal crop (Wilkinson 2000). Occupation of this area over the Holocene is episodic, and is often combined with pastoral strategies or irrigation technologies to mitigate the risk of crop failure (Smith *et al.* 2014; Wilkinson 2000; Wilkinson *et al.* 1994; 2014). However, under the right socio-ecological conditions the zone can be highly productive, and its successful exploitation has been linked to the rise of cities in the Early Bronze Age (Lawrence and Wilkinson 2015; Wilkinson *et al.* 2014) and the maintenance of empires in later periods (Wilkinson and Rayne 2010). It has also proved a useful heuristic device in the analysis of large datasets (Gaastra *et al.* 2020; Lawrence *et al.* 2021).

As Geyer *et al.* (2019) have noted, the definition of the Zone of Uncertainty is based on rainfall data, and therefore the quality of the underlying rainfall information is critical to further interpretations. They questioned the usefulness of existing maps of the zone based on precipitation maps with quite broad

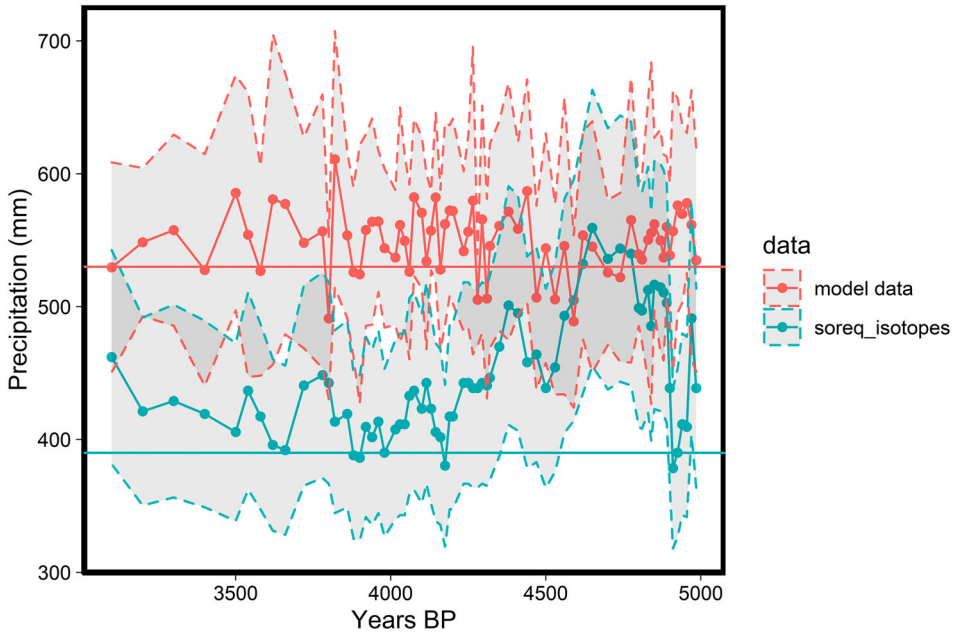


**Figure 9** **A direct comparison of the down-sampled model timeseries for precipitation and the calculated annual rainfall at Soreq Cave (data from Bar-Matthews and Ayalon 2004) for the years 5000 BP to 3000 BP. The horizontal lines show the pre-industrial value for rainfall (red), and the most recent isotope-converted rainfall value for Soreq Cave (blue).**

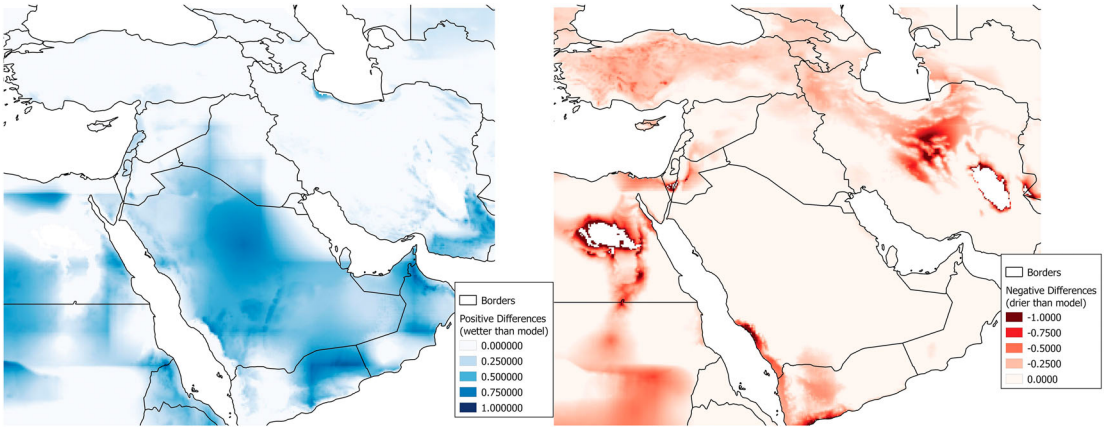


**Figure 10** **Log transformed map of differences (hindcast/model) for the year 3100 BP. Left: positive differences (hindcast was wetter than model). Right: negative differences (hindcast was drier than model). Stark white areas are locations of no-data where the original precipitation map produced zeros.**

scales (up to 1:21,000,000), especially when applied to archaeological studies on a more local scale (Geyer *et al.* 2019: 101). Here our new rainfall data is used to model the location of the Zone of Uncertainty through time. Figure 11 shows a composite image of 187 spatial reconstructions of this zone over the course of the Holocene, from 10,240 to 300 BP. These make use of the time series available from the Soreq Cave dataset, with a reconstruction for every dated point. The fuzzy edges to the Zone of Uncertainty in Fig. 11, reflect the spatial variability of the zone over time. Although this composite image shows a clear congruence that approximates where researchers might expect the Zone of Uncertainty to be located, it is somewhat misleading. There is, in fact, not a single pixel across the entire map that is consistently located in the Zone of Uncertainty throughout the Holocene from 10,240 to 300 BP.

The map series in Fig. 12 shows variability in the Zone of Uncertainty within individual millennia. As in Fig. 11, each map in Fig. 12 is a composite image of multiple reconstructions based on the new rainfall data and Soreq Cave values. The number (n) of reconstructions is displayed in the lower left corner. Composite images with more reconstructions

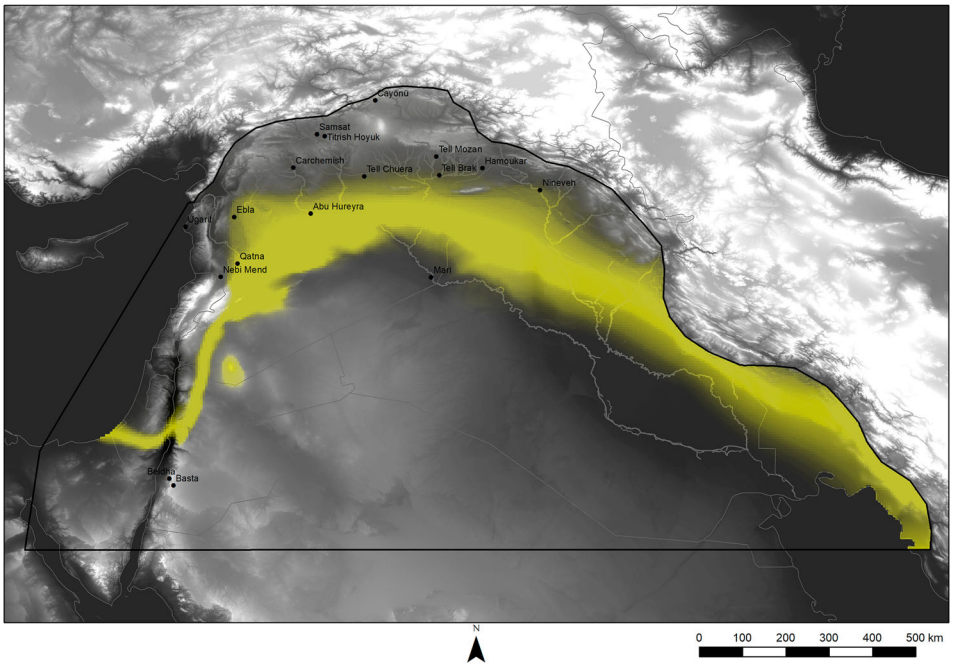


**Figure 11 A composite image of the location of the Zone of Uncertainty (10,240–300 BP).**

(higher n values) show greater inconsistency in the location of the Zone of Uncertainty (thinner bands of black). The lack of a black band in some of the maps (e.g., the 6th millennium BP) identifies millennia where variability is so great that no pixels are consistently within the Zone of Uncertainty. Figure 12 also illustrates the gradual northward migration of the Zone of Uncertainty over time from the 10th millennium BP until the 4th millennium BP. This northward movement over time corresponds to the general trend of warming and drying of the climate over the Holocene (Brayshaw *et al.* 2011; Finné *et al.* 2011; Jones *et al.* 2019; Migowski *et al.* 2006; Staubwasser and Weiss 2006). Importantly, the relationship between changes in rainfall at Soreq Cave and the size of the Zone of Uncertainty is not linear, because rainfall is not the sole variable that determines the location and shape of rainfall isohyets, either in reality or our model. Figure 13 shows the relationship between Soreq Cave rainfall and the area of the Zone of Uncertainty. At both the upper and lower rainfall values the extent of the Zone changes substantially, but in the middle ranges the extent remains reasonably similar, but, as Fig. 12 shows, the specific location of the zone moves.

Areas with rainfall values above 300 mm have also been modelled; these are taken to represent areas consistently suitable for stable rainfed agriculture. Other variables such as elevation, slope or soil depth are not considered here; a more complex model, including a wider variety of parameters, will be presented in a future publication. However, a simple rainfall driven calculation is useful to examine broad trends in agricultural potential. Figure 14 highlights the extent of this region over time from the 10th millennium BP, when plant cultivation was already taking place, until the present day. Figure 15 shows the total area suitable for rainfed agriculture through time. As one would expect, given the general Holocene drying trend, over the long term the area suitable for rainfed agriculture decreases, but there is a high degree of variability, with greater variability detected wherever there are more datapoints.

Across Figs 12, 14 and 15, the 6th millennium BP shows the greatest variability, in part due to an anomalous data point at 5186 BP that records a particularly dry year. According to our model, this would have made rainfed agriculture impossible across most of northern Syria and all northern Iraq. Surrounding years in the decades before (5206 BP) and after (5168 and 5150 BP) are also drier. At 5206 BP, rainfed agriculture would not have been possible across most of the Khabur Triangle. At 5168 and 5150 BP, rainfed agriculture would have only been possible for the northern half of the Khabur Triangle (Leilan and Mozan, but not Tell Brak or Tell Beydar). Bar-Matthews and Ayalon (2011: 169) have previously connected this dry period, detected in the Soreq Cave speleothems, with the decline of the Uruk culture. An

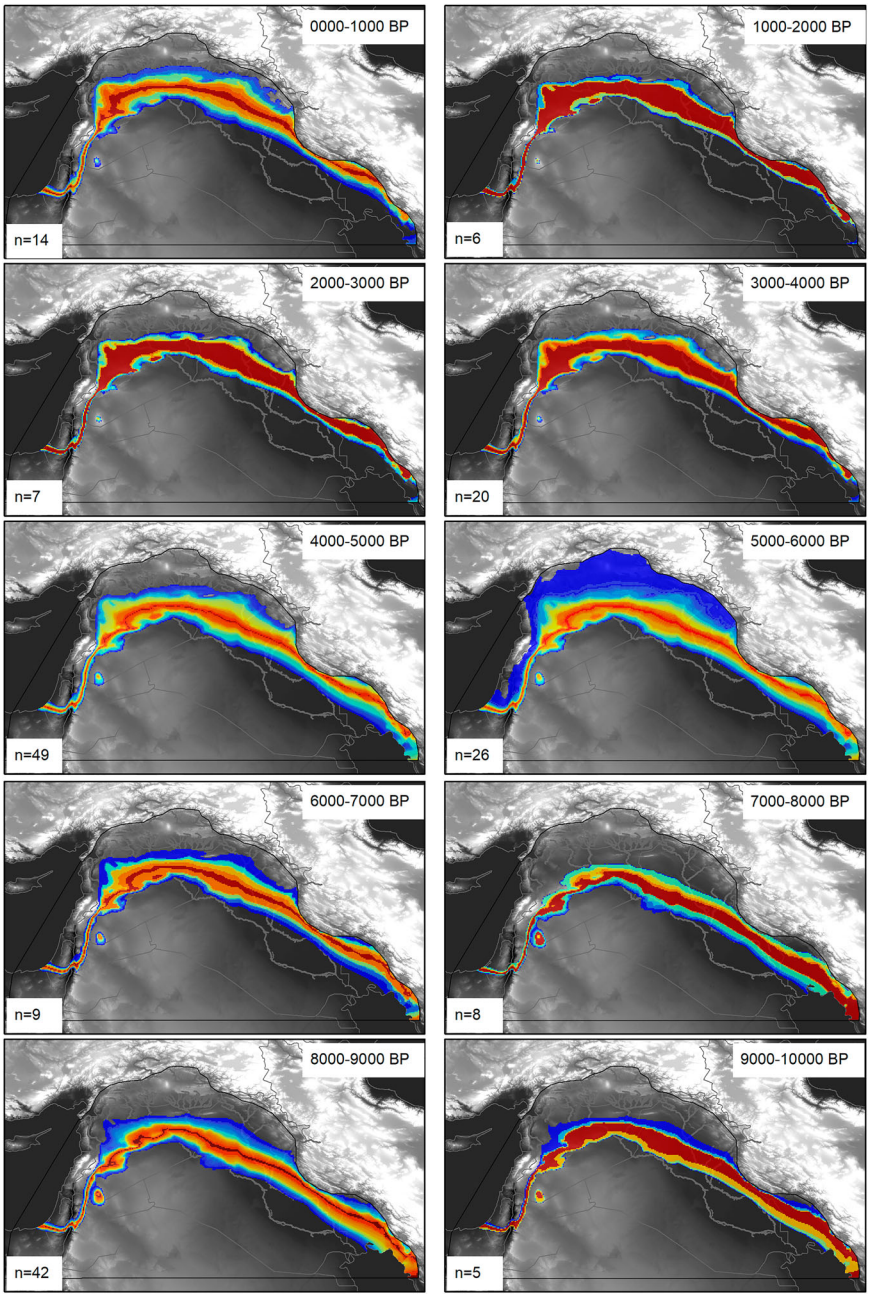


**Figure 12** **Composite images of the Zone of Uncertainty by millennium. Shades indicate the frequency with which areas are located in the Zone of Uncertainty from black (in one year) to white (all years evaluated, number of years given in lower left of image). In the 6th millennium BP, the black is absent, because not one pixel is consistently located within the Zone of Uncertainty throughout this millennium.**

analysis of settlement patterns over this span of time across the Jazira, observed that Uruk material culture and sites dominated by Uruk material culture, disappeared from the centre of the region between Tell Brak and Hamoukar by the end of the LC4 period at around 5200 BP, prior to the end of the Uruk period about 100 years later (de Gruchy 2017: 77), but the two observations are difficult to align. The settlement patterns are dated using pottery typologies and do not have the same precision as the rainfall data. Moreover, the new rainfall maps from the period immediately before 5206 BP (5226, 5246, 5266 and 5286 BP) indicate that the Jazira was within the zone of rainfed agriculture. Radiocarbon dates from the relevant sites would help clarify the impact of drought on late 4th millennium BC society by improving the ability to match settlement patterns to rainfall data.

The single rainfall map for the 11th millennium BP (10,240 BP) enables us to map where rainfed

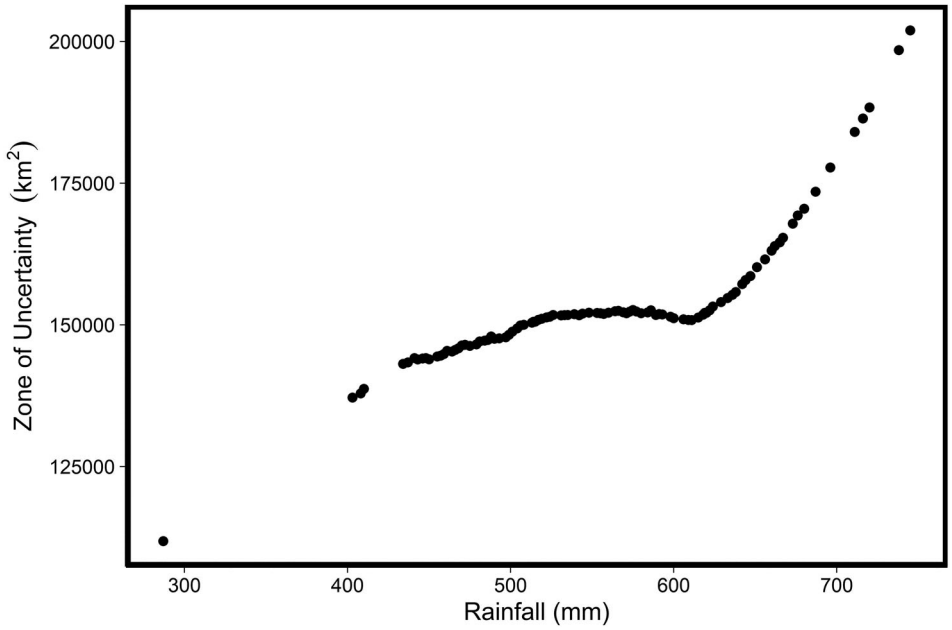


**Figure 13 The relative size of the Zone of Uncertainty in relation to rainfall values. The relationship is not linear.**

agriculture would have been possible at a time when early cultivation was taking place at various sites across the region, and important crop plants, such as wheat and lentils, were being domesticated (Asouti and Fuller 2013; Fuller *et al.* 2011). With a single data point, it is impossible to map variation in this zone, as with other millennia, but this single map makes it clear that most known early cultivation sites, including Abu Hureyra, would have been within the zone where rainfed agriculture was possible (Fig. 16). The three exceptions are Zahrat adh Dhra, Beidha and Basta in the southern Levant. This snapshot at 10,240 BP supports the general idea that cultivation could have been opportunistic and flexible (Asouti and Fuller 2013: 328), as these staple foods would have sufficient rainfall to grow without any additional water required.

The variability shown in Figs 12–15 demonstrate the importance and significance of consulting all rainfall data available for an archaeological period of interest. Even at sites where radiometric dating techniques are routinely used to constrain periodization based on ceramic typologies, phases can span ranges of at least several decades, and sometimes hundreds of years. As the values around 5.2kya BP show, the differences in rainfall over a 40-year time span can be extreme. Moreover, there is a positive correlation in Figs 13 and 15 between the number of data points and the variability detected. This means that where fewer data points are available caution should be exercised when making interpretations. In using the data made available in the Supplemental Material, we recommend users present the range of values across the period they are interested in, as well as an average value. We have also provided averaged values by millennium which can be used for long-term studies.

## Conclusion

Precipitation data is critical for fully understanding human-environment interaction. Here a new model for calculating modern rainfall in Southwest Asia, using a zonal approach to interpolate rain gauge station data has been described. We then use published precipitation shifts calculated from isotopic analysis of speleothems at Soreq Cave to hindcast the modern data from 10,240 to 300 BP, resulting in 187 irregularly spaced snapshots of past rainfall. To help assess the results, we used a Global Circulation Model for the years 5000–3000 BP and compared the precipitation output to our rainfall maps to find out which areas gave the closest values. This new rainfall map series provides a first glimpse of what is possible from speleothem data. It is hoped that in the future absolute precipitation values will become available from caves in other parts of the region, such as Kurdistan and the Arabian Peninsula. Although the SISAL database (Comas-Bru *et al.* 2020) currently contains 41 speleothem entities for 20 sites across the Middle East region, the variability between speleothems has been shown to be both high and inconsistent throughout time, with heterogeneity increasing during particular climatic periods, such as the end of Sapropel 1 at ~8kya BP (Burstyn *et al.* 2019). This

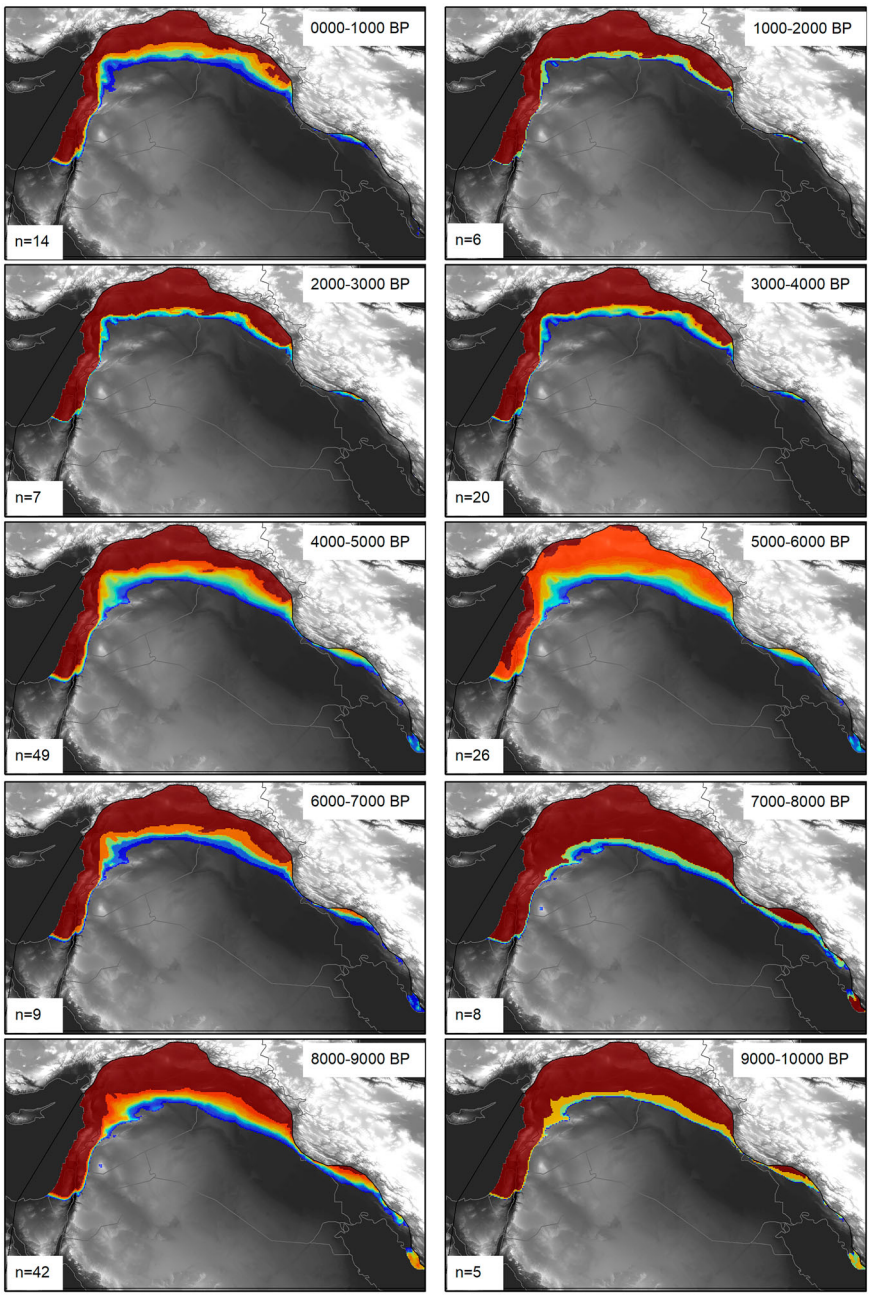


**Figure 14** **Composite images showing the locations where rainfed agriculture would have been possible during each millennium BP. The shades indicate the frequency with which areas suitable for rainfed agriculture during each millennium from white (in one year) to black (all years evaluated, n).**

is also seen in lake and marine records (Finné *et al.* 2019). The Soreq Cave data is also directly related to variability in sea surface isotope content of the Eastern Mediterranean Sea, and so does not reflect regions where rainwater is sourced from elsewhere. Additional precipitation datasets would enable a better understanding of the relationships between different proxy archives, including sea surface temperatures. This in turn would contribute to the understanding of precipitation–isotope relationships at individual cave sites and the extent to which these can be projected spatially. Interpolating between proportional changes in precipitation levels derived from multiple speleothems spread across the study region would likely improve the accuracy of our hindcast dataset.

The rainfall map series presented here can serve as a baseline dataset for use by Holocene researchers working in Southwest Asia, including archaeologists, to better understand the environmental conditions and variability specific to the periods they are studying. As new data from natural archives,

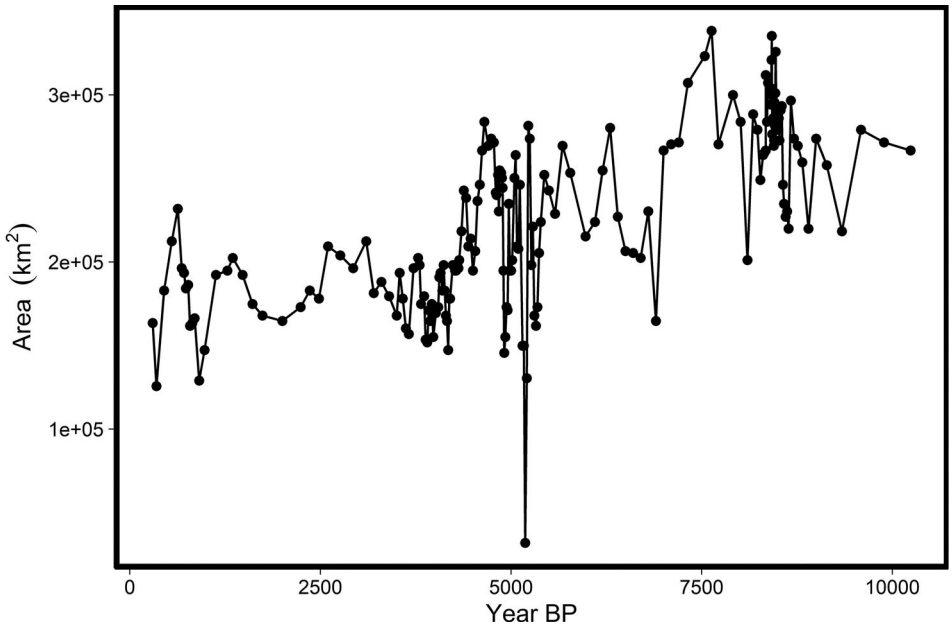


**Figure 15** **The area suitable for rainfed agriculture plotted by year. Variability is positively correlated to the number of data points available.**

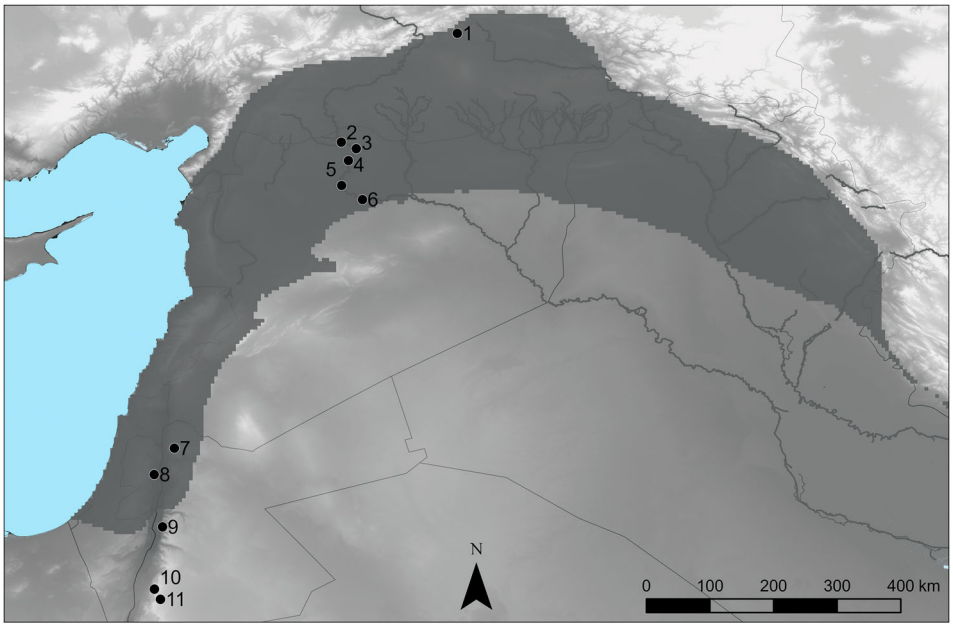


**Figure 16** **Early cultivation sites are located within the area that would have supported rainfed agriculture at precisely 10,240 BP with the exception of three sites in the southern Levant. 1—Cayönü, 2—Tell Abr, 3—Djade, 4—Tell Halula, 5—Mureybet, 6—AbuHureyra, 7—Iraq ed-Dubb, 8—Netiv Hagdud, 9—Zahrat Adh Dhra, 10—Beidha, 11—Basta.**

such as speleothems, and climate modelling projects become available they can be refined and further temporally constrained. Our diachronic analyses of the Zone of Uncertainty and land suitable for rainfed agriculture demonstrate that in the dryland environments which characterize much of the study region, relatively small shifts in rainfall can have major impacts in spatial patterning of moisture availability. As such, it is strongly recommended that users consider rainfall maps before and after the specific year(s) of interest sufficient to account for error margins within their own dataset(s), and

provide ranges and averages where appropriate in publications. This will ensure that interpretations of past phenomena which rely on land use, productivity or environmental variables are built on more solid foundations.

## Acknowledgements

This research was supported by the European Research Council under the European Union's Horizon 2020 research and innovation program for the project 'CLaSS — Climate, Landscape, Settlement and Society: Exploring Human Environment Interaction in the Ancient Near East' (grant number 802424, award holder: Dan Lawrence). ZH was also supported by the UK National Environmental Research Council (NERC) through the Research Experience Placement (REP) scheme. The climate model simulations were undertaken on ARC4, part of the High Performance Computing facilities at the University of Leeds, UK.

## Data availability statement

The R code and data outlined in this article are made available in the Supplemental Material, with exception of the rain gauge station data which can be found at ftp://opendata.dwd.de/climate_environment/CDC/observations_global/CLIMAT/multi_annual/precipitation_total/1961_1990.txt (multi-annual climate normals), ftp://opendata.dwd.de/climate_environment/CDC/observations_global/CLIMAT/monthly/qc/precipitation_total/historical/ (historical monthly totals), https://data.un.org/Data.aspx?q = precipitation&d = CLINO&f = ElementCode%3a06%3bCountryCode%3aAJ%2cAR%2cB1%2cCY%2cE1%2cGA%2cIR%2cIS%2cKW%2cKZ%2cLB%2cOM%2cPK%2cQR%2cSD%2cSU%2cSY%2cTJ%2cTU%2cTX%2cUB%2cUZ%3bStatisticCode%3a03%2c15%2c98&c = 2,5,6,7,10,15,18,19,20,22,24,26,28,30,32,34,36,38,40,42,44,46&s = CountryName:asc,WmoStationNumber:asc,StatisticCode:asc&v = 1 (WMO station data). The R code and additional supplemental data are available on Zenodo in the CLaSS Project repository, DOI: 10.5281/zenodo.5997698.

## Supplemental material

Supplemental material for this article can be accessed here: https://doi.org/10.1080/00758914.2022.2052660.

## ORCID

*Zarina Hewett* http://orcid.org/0000-0002-5131-5227
*Michelle de Gruchy* http://orcid.org/0000-0002-7856-8013
*Daniel Hill* http://orcid.org/0000-0001-5492-3925
*Dan Lawrence* http://orcid.org/0000-0001-5613-1243

## References

Algaze, G. 2008. *Ancient Mesopotamia at the dawn of civilization: the evolution of an urban landscape*. Bibliovault OAI Repository, the University of Chicago Press. doi.org/10.7208/chicago/9780226013787.001.0001.

Alex, M. and Stöehr, V. 1985. *Tübinger Atlas des Vorderen Orients*. Vorderer Orient, Niederschlagsverläßlichkeit (Middle East, rainfall reliability; A IV 4–6). Wiesbaden: Reichert.

Amand, F. St., Childs, S. T., Reitz, E. J., Heller, S., Newsom, B., Rick, T. C., Sandweiss, D. H. and Wheeler, R. 2020. Leveraging legacy archaeological collections as proxies for climate and environmental research. *Proceedings of the National Academy of Sciences* 117(15): 8287–94. doi.org/10.1073/pnas.1914154117.

Asouti, E. and Fuller, D. Q. 2013. A contextual approach to the emergence of agriculture in southwest Asia: reconstructing Early Neolithic plant-food production. *Current Anthropology* 54(3): 299–345. doi.org/10.1086/670679.

Babu, C. A., Samah, A. A. and Hamza, V. 2011. Rainfall climatology over Middle East region and its variability. *International Journal of Water Resources and Arid Environments* 1(3): 180–92.

Bar-Matthews, M. and Ayalon, A. 2004. Speleothems as palaeoclimate indicators, a case study from Soreq Cave located in the eastern Mediterranean region, Israel. In, Battarbee, R. W., Gasse, F. and Stickley, C. E., *Past Climate Variability through Europe and Africa*: 363–91. Dordrecht: Kluwer Academic Publishers.

——— 2011. Mid-Holocene climate variations revealed by high-resolution speleothem records from Soreq Cave, Israel and their correlation with cultural changes. *The Holocene* 21(1): 163–71. doi.org/10.1177/0959683610384165.

Bar-Matthews, M., Ayalon, A. and Kaufman, A. 1997. Late Quaternary paleoclimate in the eastern Mediterranean region from stable isotope analysis of speleothems at Soreq Cave, Israel. *Quaternary Research* 47(2): 155–68. doi.org/10.1006/qres.1997.1883.

——— 1998. Middle to Late Holocene (6,500 yr. period) paleoclimate in the eastern Mediterranean region from stable isotopic composition of speleothems from Soreq Cave, Israel. In, Issar, A. S. and Brown, N. (eds), *Water, Environment and Society in Times of Climatic Change: Contributions from an International Workshop within the Framework of International Hydrological Program (IHP) UNESCO, Held at Ben-Gurion University, Sede Boker, Israel from 7–12 July 1996*: 203–14. Water Science and Technology Library. Dordrecht: Springer Netherlands. doi.org/10.1007/978-94-017-3659-6_9.

——— 2000. Timing and hydrological conditions of sapropel events in the eastern Mediterranean, as evident from speleothems, Soreq Cave, Israel. *Chemical Geology* 169(1): 145–56. doi.org/10.1016/S0009-2541(99)00232-6.

Blunier, T., Chappellaz, J. Schwander, J., Stauffer, B. and Raynaud, D. 1995. Variations in atmospheric methane concentration during the Holocene epoch. *Nature* 374(6517): 46–49. doi.org/10.1038/374046a0.

Borisov, A. A. 1965. *Climates of the U.S.S.R*. Edited by Cyril A. Halstead. Translated by R. A. Ledward. Foreword by Chauncy D. Harris. Chicago: Aldine Pub. Co.

Brayshaw, D. J., Rambeau, C. M. C. and Smith, S. J. 2011. Changes in Mediterranean climate during the Holocene: insights from global and regional climate modelling. *The Holocene* 21(1): 15–31. doi.org/10.1177/0959683610377528.

Burstyn, Y., Martrat, B., Lopez, J. F., Iriarte, E., Jacobson, M. J., Lone, M. A. and Deininger, M. 2019. Speleothems from the Middle East: an example of water limited environments in the SISAL database. *Quaternary* 2(2): 16. doi.org/10.3390/quat2020016.

Chapman, L. and Thornes, J. E. 2003. The use of geographical information systems in climatology and meteorology. *Progress in Physical Geography: Earth and Environment* 27(3): 313–30. doi.org/10.1191/0309133303pp384ra.

Cheng, H., Sinha, A., Verheyden, S., Nader, F. H., Li, X. L., Zhang, P. Z., Yin, J. J., Yi, L., Peng, Y. B., Rao, Z. G., Ning, Y. F. and

Edwards, R. L. 2015. The climate variability in northern Levant over the past 20,000 years. *Geophysical Research Letters* 42(20): 8641–50. doi.org/10.1002/2015GL065397.

Clarke, J., Brooks, N., Banning, E. B., Bar-Matthews, M., Campbell, S., Cremaschi, L. C. M., di Lernia, S., Drake, N., Gallinaro, M., Manning, S., Nicoll, K., Philip, G., Rosen, S., Schoop, U.-D., Tafuri, M. A., Weninger, B. and Zerboni, A. 2016. Climatic changes and social transformations in the Near East and north Africa during the 'long' 4th millennium BC: a comparative study of environmental and archaeological evidence. *Quaternary Science Reviews* 136(March): 96–121. Special Issue: Mediterranean Holocene Climate, Environment and Human Societies. doi.org/10.1016/j.quascirev.2015.10.003.

Comas-Bru, L., Atsawawaranunt, K., Harrison, S. and SISAL working group members. 2020. SISAL (Speleothem Isotopes Synthesis and AnaLysis Working Group) Database Version 2.0. University of Reading. doi.org/10.17864/1947.256.

Cookson, E., Hill, D. J. and Lawrence, D. 2019. Impacts of long-term climate change during the collapse of the Akkadian Empire. *Journal of Archaeological Science* 106(June): 1–9. doi.org/10.1016/j.jas.2019.03.009.

Dalfes, H. N. 1997. Environmental vulnerability of early societies: some reflections on modeling issues. In, Dalfes, H. N., Kukla, G. and Weiss, H. (eds), *Third Millennium BC Climate Change and Old World Collapse*: 691–97. NATO ASI Series. Berlin, Heidelberg: Springer. doi.org/10.1007/978-3-642-60616-8_31.

Dean, J. R., Jones, M., Leng, M., Metcalfe, S. E., Sloane, H. J., Eastwood, W. J. and Roberts, N. 2018. Seasonality of Holocene hydroclimate in the eastern Mediterranean reconstructed using the oxygen isotope composition of carbonates and diatoms from Lake Nar, Central Turkey. *The Holocene* 28(2): 267–76. doi.org/10.1177/0959683617721326.

deMenocal, P., Ortiz, J., Guilderson, T. and Sarnthein, M. 2000. Coherent high- and low-latitude climate variability during the Holocene warm period. *Science* 288(5474): 2198–202. doi.org/10.1126/science.288.5474.2198.

DWD Climate Data Center. 2017a. Data set: Climatological monthly means of precipitation totals covering the period 1961–1990 (monthly normals) for stations worldwide. Version qcV001. Deutscher Wetterdienst.

——— 2017b. Data set: *Historical Dataset: Monthly Precipitation Total for Stations Worldwide*. Version qcV002. Deutscher Wetterdienst

Eastwood, W. J., Leng, M. J., Roberts, N. and Davis, B. 2007. Holocene climate change in the eastern Mediterranean region: a comparison of stable isotope and pollen data from Lake Gölhisar, southwest Turkey. *Journal of Quaternary Science* 22(4): 327–41. doi.org/10.1002/jqs.1062.

Faust, A. and Yosef Ashkenazy, Y. 2007. Excess in precipitation as a cause for settlement decline along the Israeli coastal plain during the third millennium BC. *Quaternary Research* 68(1): 37–44. doi.org/10.1016/j.yqres.2007.02.003.

Fick, S. E. and Hijmans, R. J. 2017. WorldClim 2: new 1-Km spatial resolution climate surfaces for global land areas. *International Journal of Climatology* 37(12): 4302–15. doi.org/10.1002/joc.5086.

Finné, M., Holmgren, K., Sundqvist, H. S., Weiberg, E. and Lindblom, E. 2011. Climate in the eastern Mediterranean, and adjacent regions, during the Past 6000 years — a review. *Journal of Archaeological Science* 38(12): 3153–73. doi.org/10.1016/j.jas.2011.05.007.

Finné, M., Woodbridge, J., Labuhn, I. and Roberts, N. 2019. Holocene hydro-climatic variability in the Mediterranean: a synthetic multi-proxy reconstruction. *The Holocene* 29(5): 847–63. doi.org/10.1177/0959683619826634.

Fleitmann, D., Burns, S. J., Mangini, A., Mudelsee, M., Kramers, J., Villa, I., Neff, U., Al-Subbary, A. A., Buettner, A., Hippler, D. and Matter, A. 2007. Holocene ITCZ and Indian monsoon dynamics recorded in stalagmites from Oman and Yemen (Socotra). *Quaternary Science Reviews* 26(1): 170–88. doi.org/10.1016/j.quascirev.2006.04.012.

Flückiger, J., Monnin, E., Stauffer, B., Schwander, J., Stocker, T. F., Chappellaz, J., Raynaud, D. and Barnola, J.-M. 2002. High-resolution Holocene N2O ice core record and its relationship with CH4 and CO2. *Global Biogeochemical Cycles* 16(1): 10–18.

Fohlmeister, J., Voarintsoa, N. R. G., Lechleitner, F. A., Boyd, M., Brandtstätter, S., Jacobson, M. J. and Oster, J. L. 2020. Main controls on the stable carbon isotope composition of speleothems. *Geochimica et Cosmochimica Acta* 279(June): 67–87. doi.org/10.1016/j.gca.2020.03.042.

Forte, A. M., Whipple, K. X., Bookhagen, B. and Rossi, M. W. 2016. Decoupling of modern shortening rates, climate, and topography in the Caucasus. *Earth and Planetary Science Letters* 449 (September): 282–94. doi.org/10.1016/j.epsl.2016.06.013.

Fuks, D., Ackermann, O., Ayalon, A., Bar-Matthews, M., Bar-Oz, G., Levi, Y., Maeir, A. M., Weiss, E., Zilberman, T. and Safrai, Z. 2017. Dust clouds, climate change and coins: consiliences of palaeoclimate and economy in the Late Antique southern Levant. *Levant* 49(2): 205–23. doi.org/10.1080/00758914.2017.1379181.

Fuller, D., Willcox, G. and Allaby, R. 2011. Early agricultural pathways: moving outside the 'core area' hypothesis in southwest Asia. *Journal of Experimental Botany* 63(2): 617–33. doi.org/10.1093/jxb/err307.

Gaastra, J. S., Greenfield, T. L. and Greenfield, H. J. 2020. Constraint, complexity and consumption: zooarchaeological meta-analysis shows regional patterns of resilience across the Metal Ages in the Near East. *Quaternary International*, ArchaeoLife and Environment, 545(April): 45–62. doi.org/10.1016/j.quaint.2019.03.013.

Geyer, B., Braemer, F., Davtian, G. and Philip, G. 2019. A geo-archaeological approach to the study of hydro-agricultural systems in arid areas of western Syria. *Journal of Arid Environments* 163(April): 99–113. doi.org/10.1016/j.jaridenv.2018.11.005.

Göktürk, O. M., Fleitmann, D., Badertscher, S., Cheng, H., Edwards, R. L., Leuenberger, M., Fankhauser, A., Tüysüz, O. and Kramers, J. 2011. Climate on the southern Black Sea coast during the Holocene: implications from the Sofular Cave record. *Quaternary Science Reviews* 30(19): 2433–45. doi.org/10.1016/j.quascirev.2011.05.007.

Goovaerts, P. 2000. Geostatistical approaches for incorporating elevation into the spatial interpolation of rainfall. *Journal of Hydrology* 228(1): 113–29. doi.org/10.1016/S0022-1694(00)00144-X.

Groucutt, H. S., Breeze, P. S., Guagnin, M., Stewart, M., Drake, N., Shipton, C., Zahrani, B., Al Omarfi, A., Alsharekh, A. M. and Petraglia, M. D. 2020. Monumental landscapes of the Holocene humid period in northern Arabia: the Mustatil Phenomenon. *The Holocene* 30(12): 1767–79. doi.org/10.1177/0959683620950449.

Gruchy, M. de. 2017. Routes of the Uruk expansion. PhD. University of Durham.

Hijmans, R. J., Cameron, S. E., Parra, J. L., Jones, P. G. and Jarvis, A. 2005. Very high-resolution interpolated climate surfaces for global land areas. *International Journal of Climatology* 25(15): 1965–78. doi.org/10.1002/joc.1276.

Huffman, G. J., Adler, R. F., Bolvin, D. T. and Nelkin, E. J. 2010. The TRMM multi-satellite precipitation analysis (TMPA). In, Gebremichael, M. and Hossain, F. (eds), *Satellite Rainfall Applications for Surface Hydrology*: 3–22. Dordrecht: Springer Netherlands. doi.org/10.1007/978-90-481-2915-7_1.

Huffman, G. J., Bolvin, D. T., Nelkin, E. J., Wolff, D. B., Adler, R. F., Yang Hong, G. G., Bowman, K. P. and Stocker, E. F. 2007. The TRMM multisatellite precipitation analysis (TMPA): quasi-global, multiyear, combined-sensor precipitation estimates at fine scales. *Journal of Hydrometeorology* 8(1): 38–55. doi.org/10.1175/JHM560.1.

Iyigun, C., Türkeş, M., Batmaz, I., Yozgatligil, C., Purutçuoğlu, V., Koc, E. and Ozturk, M. Z. 2013. Clustering current climate regions of Turkey by using a multivariate statistical method. *Theoretical and Applied Climatology* 114(January): 95–106. doi.org/10.1007/s00704-012-0823-7.

Jacquin, A. and Soto-Sandoval, J. 2013. Interpolation of monthly precipitation amounts in mountainous catchments with sparse precipitation networks. *Chilean Journal of Agricultural Research* 73 (December): 406–13. doi.org/10.4067/S0718-58392013000400012.

Javanmard, S., Yatagai, A., Nodzu, M. I., BodaghJamali, J. and Kawamoto, H. 2010. Comparing high-resolution gridded precipitation data with satellite rainfall estimates of TRMM_3B42 over Iran. *Advances in Geosciences* 25: 119–25. doi.org/10.5194/adgeo-25-119-2010, 2010.

Jennings, R. P., Singarayer, J., Stone, E. J., Krebs-Kanzow, U., Khon, V., Nisancioglu, K. H., Pfeiffer, M., Zhang, X., Parker, A.,

Parton, A., Groucutt, H. S., White, T. S., Drake, N. A. and Petraglia, M. D. 2015. The greening of Arabia: multiple opportunities for human occupation of the Arabian peninsula during the Late Pleistocene inferred from an ensemble of climate model simulations. *Quaternary International*, Green Arabia: human prehistory at the cross-roads of continents, 382(September): 181–99. doi.org/10.1016/j.quaint.2015.01.006.

Jones, M. D., Abu-Jaber, N., Al Shdaifat, A., Baird, D., Cook, B. I., Cuthbert, M. O., Dean, J. R., et al. 2019. 20,000 years of societal vulnerability and adaptation to climate change in southwest Asia. *WIREs Water* 6(2): e1330. doi.org/10.1002/wat2.1330.

Kalayci, T. 2013. Agricultural production and stability of settlement systems in Upper Mesopotamia during the Early Bronze Age (third millennium BCE). PhD. University of Arkansas.

Kaniewski, D., Van Campo, E. and Weiss, H. 2012. Drought is a recurring challenge in the Middle East. *Proceedings of the National Academy of Sciences* 109(10): 3862–67. doi.org/10.1073/pnas.1116304109.

Kaniewski, D., Guiot, J. and Van Campo, E. 2015. Drought and societal collapse 3200 years ago in the eastern Mediterranean: a review. *WIREs Climate Change* 6(4): 369–82. doi.org/10.1002/wcc.345.

Kaufman, A., Wasserburg, G. J., Porcelli, D., Bar-Matthews, M., Ayalon, A. and Halicz, L. 1998. U-Th isotope systematics from the Soreq Cave, Israel and climatic correlations. *Earth and Planetary Science Letters* 156(3): 141–55. doi.org/10.1016/S0012-821X(98)00002-8.

Kennett, D. J. and Kennett, J. P. 2006. Early state formation in southern Mesopotamia: sea levels, shorelines, and climate change. *The Journal of Island and Coastal Archaeology* 1(1): 67–99. doi.org/10.1080/15564890600586283.

Khalili, A. and Rahimi, J. 2014. High-resolution spatiotemporal distribution of precipitation in Iran: a comparative study with three global-precipitation datasets. *Theoretical and Applied Climatology* 118(1): 211–21. doi.org/10.1007/s00704-013-1055-1.

Kirleis, W. and Herles, M. 2007. Climatic change as a reason for Assyro-Aramaean conflicts? Pollen evidence for drought at the end of the 2nd millennium BC. *State Archives of Assyria, Bulletin* 16 (January): 7–37.

Kuzucuoğlu, C. and Marro, C. 2007. Sociétés humaines et changement climatique à la fin du troisième millénaire: une crise a-t-elle eu lieu en Haute-Mésopotamie?: Actes du colloque de Lyon, 5–8 décembre 2005. Varia Anatolica 19. Institut français d'études anatolienne Georges-Dumézil.

Kyriakidis, P. C., Kim, J. and Miller, N. L. 2001. Geostatistical mapping of precipitation from rain gauge data using atmospheric and terrain characteristics. *Journal of Applied Meteorology* 40(11): 1855–77. doi.org/10.1175/1520-0450(2001)040 < 1855:GMOPFR>2.0.CO;2.

Laskar, J., Robutel, P., Joutel, F., Gastineau, M., Correia, A. C. M. and Levrard, B. 2004. A long-term numerical solution for the insolation quantities of the earth. *Astronomy & Astrophysics* 428(1): 261–85. doi.org/10.1051/0004-6361:20041335.

Lawrence, D. and Wilkinson, T. J. 2015. Hubs and upstarts: pathways to urbanism in the Northern Fertile Crescent. *Antiquity* 89(344): 328–44. doi.org/10.15184/aqy.2014.44.

Lawrence, D., Philip, G., Hunt, H., Snape-Kennedy, L. and Wilkinson, T. J. 2016. Long Term Population, City Size and Climate Trends in the Fertile Crescent: A First Approximation. *PLOS ONE* 11 (3): e0152563. doi.org/10.1371/journal.pone.0152563.

Lawrence, D., Philip, G., Wilkinson, K., Buylaert, J.-P., Murray, A. S., Thompson, W. and Wilkinson, T. J. 2017. Regional power and local ecologies: accumulated population trends and human impacts in the Northern Fertile Crescent. *Quaternary International* 437: 60–81.

Lawrence, D., de Gruchy, M. and Palmisano, A. 2021. Collapse and continuity: a multi-proxy reconstruction of settlement organization and population trajectories in the northern Fertile Crescent during the 4.2kya rapid climate change event. PLOS ONE 16, e0244871. doi.org/10.1371/journal.pone.0244871.

Maher, L. A., Banning, E. B. and Chazan, M. 2011. Oasis or mirage? Assessing the role of abrupt climate change in the prehistory of the southern Levant. *Cambridge Archaeological Journal* 21(1): 1–30. doi.org/10.1017/S0959774311000011.

Migowski, C., Stein, M., Prasad, S., Negendank, J. F. W. and Agnon, A. 2006. Holocene Climate variability and cultural evolution in the Near East from the Dead Sea sedimentary record. *Quaternary Research* 66(3): 421–31. doi.org/10.1016/j.yqres.2006.06.010.

Mmbando, G. A. and Kleyer, M. 2018. Mapping precipitation, temperature, and evapotranspiration in the Mkomazi River Basin, Tanzania. *Climate* 6(3). doi.org/10.3390/cli6030063.

Monnin, E., Steig, E. J., Siegenthaler, U., Kawamura, K., Schwander, J., Stauffer, B., Stocker, T. F., Morse, D. L., Barnola, J.-M., Bellier, B., Raynaud, D. and Fischer, H. 2004. Evidence for substantial accumulation rate variability in Antarctica during the Holocene, through synchronization of $CO_2$ in the Taylor Dome, Dome C and DML ice cores. *Earth and Planetary Science Letters* 224(1): 45–54. doi.org/10.1016/j.epsl.2004.05.007.

New, M., Hulme, M. and Jones, P. 1999. Representing twentieth-century space–time climate variability. Part I: development of a 1961–90 mean monthly terrestrial climatology. *Journal of Climate* 12: 829–56. doi.org/10.1175/1520-0442(1999)012< 0829:RTCSTC>2.0.CO;2.

Orland, I. J., Bar-Matthews, M., Kita, N. T., Ayalon, A., Matthews, A. and Valley, J. W. 2009. Climate deterioration in the eastern Mediterranean as revealed by ion microprobe analysis of a speleothem that grew from 2.2 to 0.9 Ka in Soreq Cave, Israel. *Quaternary Research* 71(1): 27–35. doi.org/10.1016/j.yqres.2008.08.005.

Orland, I. J., Bar-Matthews, M., Ayalon, A., Matthews, A., Kozdon, R., Ushikubo, T. and Valley, J. W. 2012. Seasonal resolution of eastern Mediterranean climate change since 34ka from a Soreq Cave speleothem. *Geochimica et Cosmochimica Acta* 89(July): 240–55. doi.org/10.1016/j.gca.2012.04.035.

Orland, I. J., Burstyn, Y., Bar-Matthews, M., Kozdon, R., Ayalon, A., Matthews, A. and Valley. J. W. 2014. Seasonal climate signals (1990–2008) in a modern Soreq Cave stalagmite as revealed by high-resolution geochemical analysis. *Chemical Geology* 363 (January): 322–33. doi.org/10.1016/j.chemgeo.2013.11.011.

Orland, I. J., He, F., Bar-Matthews, M., Chen, G., Ayalon, A. and Kutzbach, J. E. 2019. Resolving seasonal rainfall changes in the Middle East during the last interglacial period. *Proceedings of the National Academy of Sciences* 116(50): 24985. doi.org/10.1073/pnas.1903139116.

Orlovsky, N. S. 1994. Climate of Turkmenistan. In, Fet, V. and Atamuradov, K. I. (eds), *Biogeography and Ecology of Turkmenistan*: 23–48. Dordrecht: Springer Netherlands. doi.org/10.1007/978-94-011-1116-4_3.

Palmisano, A., Lawrence, D., de Gruchy, M., Bevan, A. and Shennan, S. 2021. Holocene regional population dynamics and climatic trends in the Near East: a first comparison using archaeo-demographic proxies. *Quaternary Science Reviews* 252: 106739.

Patlakas, P., Stathopoulos, C., Flocas, H., Kalogeri, C. and Kallos, G. 2019. Regional climatic features of the Arabian Peninsula. *Atmosphere* 10(4). doi.org/10.3390/atmos10040220.

Pfälzner, P. 2002. Modes of storage and the development of economic systems in the early Jezireh-period. In, Al-Gairani Weer, L., Curtis, J. Martin, H. McMahon, A., Oates, J and Reade, J. (eds), *Of Pots and Plans: Papers on the Archaeology and History of Mesopotamia and Syria presented to David Oates in Honour of his 75th Birthday*: 259–86. London: Nabu. doi.org/10.11588/propylaeumdok.00003418.

Rayne, L. 2014. Water and territorial Empires. PhD. University of Durham.

Schneider, U., Becker, A., Finger, P., Meyer-Christoffer, A. and Ziese, M. 2018. GPCC full data monthly product version 2018 at 0.25°: monthly land-surface precipitation from rain-guages built on GTS-based and historical data. Electronic dataset. Global Precipitation Climatology Centre (GPCC, http://gpcc.dwd.de/) at Deutscher Wetterdienst doi.org/10.5676/DWD_GPCC/FD_M_V2018_025

Sensoy, S. and Demircan, M., Ulupinar, Y. and Balta, I. 2008. Climate of turkey. *Turkish state meteorological service*, *401*.

Smith, S., Wilkinson, T. and Lawrence, D. 2014. Agro-pastoral landscapes in the zone of uncertainty: the Middle Euphrates and north Syrian Steppe during the 4th and 3rd millennia BC. In, Morandi Bonacossi, D. (ed.), *Settlement Dynamics and Human-Landscape Interaction in the Dry Steppes of Syria*: 151–72. Studia Chaburiensa 4. Wiesbaden: Harrassowitz.

Staubwasser, M. and Weiss, H. 2006. Holocene climate and cultural evolution in late prehistoric–early historic West Asia. *Quaternary Research* 66(3): 372–87. doi.org/10.1016/j.yqres.2006.09.001.

Stevens, L. R., Ito, E., Schwalb, A. and Wright, H. E. 2006. Timing of atmospheric precipitation in the Zagros Mountains inferred from a multi-proxy record from Lake Mirabad, Iran. *Quaternary Research* 66(3): 494–500. doi.org/10.1016/j.yqres.2006.06.008.

Subyani, A. M. 2004. Geostatistical study of annual and seasonal mean rainfall patterns in southwest Saudi Arabia/distribution géostatistique de la pluie moyenne annuelle et saisonnière dans le Sud-Ouest de l'Arabie Saoudite. *Hydrological Sciences Journal* 49(5): 803–17. doi.org/10.1623/hysj.49.5.803.55137.

Sun, F., Roderick, M. L. and Farquhar, G. D. 2018. Rainfall statistics, stationarity, and climate change. *Proceedings of the National Academy of Sciences* 115(10): 2305–10. doi.org/10.1073/pnas.1705349115.

Thomas, A. and Herzfeld, U. C. 2004. REGEOTOP: new climatic data fields for East Asia based on localized relief information and geostatistical methods. *International Journal of Climatology* 24(10): 1283–306. doi.org/10.1002/joc.1058.

Ur, J. A. 2010. Cycles of civilization in northern Mesopotamia, 4400–2000 BC. *Journal of Archaeological Research* 18(4): 387–431. doi.org/10.1007/s10814-010-9041-y.

Ur, J. 2015. Urban adaptations to climate change in northern Mesopotamia. *Climate and Ancient Societies*. In, Kerner, S., Dann, R. and Bangsgaard Jensen, P. (eds), *Climate and Ancient Societies*: 69–95. Copenhagen: Museum Tusculanum Press.

Viste, E. and Sorteberg, A. 2013. Moisture transport into the Ethiopian highlands. *International Journal of Climatology* 33(1): 249–63. doi.org/10.1002/joc.3409.

Wassenaar, L. I., Terzer-Wassmuth, S., Douence, C., Araguas-Araguas, L., Aggarwal, P. K. and Coplen, T. B. 2018. Seeking excellence: an evaluation of 235 international laboratories conducting water isotope analyses by isotope-ratio and laser-absorption spectrometry. *Rapid Communications in Mass Spectrometry* 32 (5): 393–406. doi.org/10.1002/rcm.8052.

Weiss, H. 2017. Seventeen kings who lived in tents. In, Höflmayer, F. (ed.), *The Late Third Millennium in the Ancient Near East: Chronology, C14, and Climate Change*: 131–62. Oriental Institute Seminars, 11. Chicago: The Oriental Institute of the University of Chicago.

Weiss, H. and Bradley, R. S. 2001. What drives societal collapse? *Science* 291(5504): 609–10. doi.org/10.1126/science.1058775.

Weiss, H., Courty, H.-A., Wetterstrom, W., Guichard, F., Senior, L., Meadow, R. and Curnow, A. 1993. The genesis and collapse of third millennium north Mesopotamian civilization. *Science* 261 (5124): 995–1004. doi.org/10.1126/science.261.5124.995.

Wilkinson, T. J. 2000. Regional approaches to Mesopotamian archaeology: the contribution of archaeological surveys. *Journal of Archaeological Research* 8 (3): 219–67. doi.org/10.1023/A:1009487620969.

Wilkinson, T. J. and Rayne, L. 2010. Hydraulic landscapes and imperial power in the Near East. *Water History* 2(2): 115–44. doi.org/10.1007/s12685-010-0024-1.

Wilkinson, T. J., Bintliff, J., Curvers, H. H., Halstead, P., Kohl, P. L., Liverani, M., McCorriston, J., Oates, J., Schwartz, G. M., Thuesen, I., Weiss, H. and Courty, M.-A. 1994. The structure and dynamics of dry-farming states in Upper Mesopotamia [and comments and reply]. *Current Anthropology* 35(5): 483–520.

Wilkinson, T. J., Philip, G., Bradbury, J., Dunford, R., Donoghue, D., Galiatsatos, N., Lawrence, D., Ricci, A. and Smith, S. L. 2014. Contextualizing early urbanization: settlement cores, early states and agro-pastoral strategies in the fertile crescent during the fourth and third millennia BC. *Journal of World Prehistory* 27(1): 43–109. doi.org/10.1007/s10963-014-9072-2.

Wilson, A. M., Parmentier, B. and Jetz, W. 2014. Systematic land cover bias in collection 5 MODIS cloud mask and derived products — a global overview. *Remote Sensing of Environment* 141(February): 149–54. doi.org/10.1016/j.rse.2013.10.025.

Wolfer, W. 1984. *Vorderer Orient: Mittlere Jahresniederschläge Und Variabilität*. Tübinger Atlas Des Vorderen Orients (TAVO). Wiesbaden: Dr. Ludwig Reichert Verlag.

World Meteorological Organization (WMO). 2017. WMO Guidelines on the Calculation of Climate Normals, 2017 edition. WMO-No. 1203. Geneva: WMO.

Wossink, A. 2009. Challenging Climate Change. Competition and Cooperation among Pastoralists and Agriculturalists in Northern Mesopotamia (c. 3000–1600 BC). https://www.sidestone.com/books/challenging-climate-change.

Yasur-Landau, A., Cline, E. H. and Rowan, Y. 2018. *The Social Archaeology of the Levant: From Prehistory to the Present*. Cambridge: Cambridge University Press.

Xie, P., Arkin, P. A. 1997. Global precipitation: a 17-year monthly analysis based on gauge observations, satellite estimates, and numerical model outputs. Bulletin of American Meteorological Society 78: 2539–58. doi.org/10.1175/1520-0477(1997)078<2539:GPAYMA>2.0.CO;2.

Zohary, M. 1973. *Geobotanical Foundations of the Middle East*. Stuttgart: Fischer.